IWS1 phosphorylation by AKT kinase controls the nucleocytoplasmic export of type I IFNs and the sensitivity of lung adenocarcinoma cells to oncolytic viral infection, through *U2AF2* RNA splicing.

Georgios I. Laliotis[1,2,3,12*], Adam D. Kenney[4,5], Evangelia Chavdoula[1,2] , Arturo Orlacchio[1,2], Abdul K. Kaba[1,2], Alessandro La Ferlita[1,2,6], Vollter Anastas[1,2,7], Christos Tsatsanis[8,9], Joal D. Beane[2,10], Lalit Sehgal[11], Vincenzo Coppola[1,2] , Jacob S. Yount [4,5] and Philip N. Tsichlis[1,2,13*]

[1]The Ohio State University, Department of Cancer Biology and Genetics, Columbus, OH, 43210, [2]The Ohio State University Comprehensive Cancer Center-Arthur G. James Cancer Hospital and Richard J. Solove Research Institute, Columbus, OH, 43210, [3]University of Crete, School of Medicine, Heraklion Crete, 71500, Greece, [4]Department of Microbial Infection and Immunity, The Ohio State University, Columbus, OH, 43210, [5]Infectious Diseases Institute, The Ohio State University, Columbus, OH, 43210, [6]Department of Clinical and Experimental Medicine, Bioinformatics Unit, University of Catania, Catania, 95131, Italy, [7]Tufts Graduate School of Biomedical Sciences, Program in Genetics, Boston, MA, 02111 [8]Department of Clinical Chemistry-Biochemistry, School of Medicine, University of Crete, Heraklion 71110, Crete, Greece, [9]Institute for Molecular Biology and Biotechnology, Foundation for Research and Technology Hellas, Heraklion 70013, Greece, [10]The Ohio State University, Department of Surgery, Division of Surgical Oncology, Columbus, OH 43210 [11]College of Medicine, Department of Hematology, The Ohio State University, Columbus, OH 43210

Present Address :

[12]The Sidney Kimmel Comprehensive Cancer Center, Johns Hopkins University, Baltimore, MD, 21231

Running Title: IWS1 affects sensitivity to oncolytic viruses

[13]Lead Contact

*Correspondence should be addressed to: Philip N. Tsichlis (Philip.tsichlis@osumc.edu) and Georgios I. Laliotis (glaliot7@gmail.com)

Abstract

Type I IFNs orchestrate the antiviral response. Interestingly, *IFNA1* and *IFNB1* genes are naturally intronless. Based on previous work, the splicing factor U2 Associated Factor 65 (U2AF65), encoded by *U2AF2*, and pre-mRNA Processing factor 19 (Prp19) function on the Cytoplasmic Accumulation Region Elements (CAR-E), affecting the nuclear export of intronless genes. We have previously shown that the loss of IWS1 phosphorylation by AKT3, promotes the alternative RNA splicing of *U2AF2*, resulting in novel transcripts lacking exon 2. This exon encodes part of the Serine-Rich (RS) domain of U2AF65, which is responsible for its binding with Prp19. Here, we show that IWS1 phosphorylation and the *U2AF2* RNA splicing pattern affect the nuclear export of introless mRNAs. We also demonstrate that the same axis is required for the proper function of the CAR-Es. Mechanistically, whereas both U2AF65 isoforms bind CAR-E, the recruitment of Prp19 occurs only in cells expressing phosphorylated IWS1, promoting intronless genes' export. Moreover, analysis of Lung adenocarcinoma patients showed that high p-IWS1 activity correlates with the assembly of the U2AF65/Prp19 complex and export of intronless genes, *in vivo*. Accordingly, the expression of type I IFNs was decreased in cells deficient in IWS1 phosphorylation and the viral infection was increased. Furthermore, following infection with oncolytic virus, we observed reduced activation of p-STAT1 and expression of Interferon Stimulated Genes (ISG), in cells stimulated by shIWS1-derived supernatant, or cells treated with the pan-AKT inhibitor, MK2206. Consistently, killing curves and apoptosis assays after infection with oncolytic viruses, revealed increased susceptibility upon the loss of IWS1, with subsequent activation of Caspase-mediated death. The treatment of the lung adenocarcinoma cells with MK2206, phenocopied the loss of IWS1 phosphorylation. These data identify a novel mechanism by which the AKT/p-IWS1 axis, by hijacking the epigenetic regulation of RNA splicing and processing, contributes to the resistance to oncolytic viral infection, suggesting that combined inhibition of the splicing machinery and AKT/p-IWS1 signals would sensitize tumors to oncolytic viral treatment.

56 **Introduction**

57 Type I interferons (IFNs) are members of a large signaling family of proteins, known
58 for their robust antiviral response. Specifically, type I IFNs are encoded by 13 *IFNA* genes and
59 a single *IFNB* gene (Frisch et al., 2020[1]). These genes are rapidly induced by Pattern
60 Recognition Receptors (PRRs), the sensors of innate immunity (Acosta et al., 2020[2]). These
61 receptors recognize molecules presented by pathogens (pathogen-associated molecular
62 patterns, PAMPs), such as double-stranded RNA (dsRNA), bacterial lipopolysaccharides,
63 flagellin, bacterial lipoproteins, and cytosolic DNA. (Amarante-Mendes et al., 2018[3]). Signals
64 from PRRs converge upon IKK-family kinases to phosphorylate and activate two transcription
65 factors, IRF3 and NF-kB; these factors directly transactivate the *IFNB1* gene (Ablasser et al.,
66 2020[4]). IFNβ in an autocrine or paracrine manner and activates the IFNAR1/2 receptors,
67 resulting in Janus kinase (JAK)-mediated phosphorylation of STAT1 and STAT2, forming a
68 canonical complex of STAT1/STAT2/IRF9, known as the Interferon Stimulated Gene Factor 3
69 (ISGF3) complex. This activated complex transcribes target genes (interferon-stimulated
70 genes, ISGs) containing ISRE (ISGF3 response elements), that limit viral replication (Aleynick
71 et al., 2019[5]).

72 Activation of the type I IFN pathway is critical in antiviral immunity and in mediating a
73 wide array of innate immune responses. Modulating this pathway is not only critical for
74 controlling antiviral and inflammatory responses, but it also offers translational applications.
75 One of the most important translational applications of the activation of this pathway is the
76 usage of oncolytic viruses (OV). OVs have gained momentum in recent years because of their
77 immune-stimulating effects, both systemically and in the local tumor microenvironment (Park
78 et al., 2020[7]). The first clinically approved OV, Talimogene laherparepvec (TVEC), is a
79 genetically modified type I herpes simplex virus (HSV) that expresses granulocyte-
80 macrophage colony-stimulating factor (GM-CSF) (Rehman et al., 2016[7]). While TVEC is
81 routinely used in select patients with melanoma, most other OVs have not shown robust
82 antitumor efficacy in clinical trials, especially when used as monotherapy (Martinez-Quintanilla

83 et al., 2019[8]). Thus, deeper comprehension of the molecular pathways involved in the efficacy
84 of these therapeutic approaches is a necessity for the proper design of antitumor oncolytic
85 therapies.

86 One way to improve the response to OV therapy is through the manipulation of multiple
87 signalling pathways regulating the type I IFN response. Among them, the AKT pathway
88 regulates the IFN response at multiple levels, with many of its activities being isoform-specific.
89 Early studies have shown that by activating the mechanistic target of rapamycin (mTOR), AKT
90 promotes the translation of ISGs (Kroczynska et al., 2014[9]). Subsequent studies revealed that
91 AKT1 activates β-catenin, promoting the transcriptional activation of *IFNB1* (Gantneret al.,
92 2012[10]). In addition, we have shown that AKT1 selectively phosphorylates EMSY at S209,
93 relieving the EMSY-mediated repression of ISGs (Ezell et al., 2012[11]).

94 Interestingly, genes encoding *IFNA1* and *IFNB1* are naturally intronless (de Padilla et
95 al., 2014[12]). In contrast to splicing-dependent mRNA export, little is known regarding the
96 nuclear export of intronless mRNAs. Based on previous reports, components of the
97 Transcription-Export (TREX) complex, the pre-mRNA Processing Factor 19 (Prp19) complex
98 and the splicing factor U2 Associated-Factor 2 (U2AF2) associate with designated
99 Cytoplasmic Accumulation Region Elements (CAR-E), a 10-nt consensus element on
100 intronless genes, and function in their mRNA export (Lei et al., 2013[13]). These data suggest
101 the presence of an additional layer in the regulation of type I IFN expression.

102 Based on our previous observations, IWS1 (Interacts With Spt6) is an RNA processing
103 factor and phosphorylation target of AKT kinase at S720/T721 (Sanidas et al., 2014[14]). More
104 recently we revealed that IWS1 phosphorylation affects genome-wide the alternative RNA
105 splicing program in human lung adenocarcinoma (Laliotis et al., 2020[15]). In one example, the
106 loss of phosphorylated IWS1 resulted in a novel, exon 2 deficient splice variant of the splicing
107 factor *U2AF2.* This exon encodes part of the U2AF65 Serine-Rich (RS) Domain, which is
108 required for its binding with Prp19, further affecting the downstream splicing machinery. We
109 also provided evidence that the *U2AF2* exon 2 inclusion depends on phosphorylated IWS1,

110 by promoting histone H3K36 trimethylation by SETD2 and the assembly of LEDGF/SRSF1
111 splicing complexes, in a cell-cycle specific manner (Laliotis et al., 2020[16]).

112 Since IWS1 phosphorylation controls the U2AF65-Prp19 interaction through the
113 epigenetic regulation of *U2AF2* alternative RNA splicing, we sought to investigate the effect of
114 this pathway in the nucleocytoplasmic export of naturally intronless genes, including *IFNA1*
115 and *IFNB1.* In this study, our goal was to elucidate the molecular mechanisms, following IWS1
116 phosphorylation and the subsequent hijacking of alternative RNA splicing program, that affect
117 the nucleocytoplasmic export of intronless mRNAs and to highlight a novel role of AKT kinase
118 signaling in the regulation of type I IFN response and sensitivity of lung adenocarcinoma cells
119 to infection with oncolytic viral strains.

120 **Results**

121 **IWS1 phosphorylation regulates the nucleocytoplasmic transport of intronless gene**
122 **mRNAs, via *U2AF2* alternative RNA splicing.**

123 Our earlier studies have shown that the knockdown of IWS1 and its replacement by
124 the non-phosphorylatable mutant IWS1 S720A/T721A, altered the RNA splicing pattern of
125 *U2AF2* (Laliotis et al., 2020[15]). The predominant novel splice variant of the *U2AF2* mRNA that
126 we identified in these cells, lacks exon 2, which encodes part of the N-terminal RS domain of
127 U2AF65. This domain is responsible for the interaction of U2AF65 with Prp19, a component
128 of the seven-member ubiquitin ligase complex Prp19C (Laliotis et al., 2020[15], R. Hogg et al.,
129 2010[17], Chanarat S. et al., 2013[18]). More importantly, U2AF65 and Prp19C, along with
130 components of the TREX complex, bind elements designated as Cytoplasmic Accumulation
131 Region Elements (CAR-E) in naturally intronless mRNAs, promoting their nucleocytoplasmic
132 transport (Lei et al., 2013[13]). Examples of mRNAs whose nucleocytoplasmic transport is
133 regulated by this mechanism include *IFNA1, IFNB1, JUN and HSBP3* (Lei et al., 2013[13]).

134 Based on this knowledge, we hypothesized that IWS1 phosphorylation affects the
135 nucleocytoplasmic export of these mRNAs, through the alternative RNA splicing of *U2AF2*

136 and the U2AF65-Prp19 interaction. First, we engineered shControl, shIWS1, shIWS1/wild type
137 IWS1 rescue (shIWS1/WT-R), shIWS1/phosphorylation site IWS1 mutant rescue
138 (shIWS1/MT-R) and shIWS1/U2AF65α (exon 2-containing) or U2AF65β (exon 2-deficient)
139 rescue NCI-H522 and NCI-H1299 lung adenocarcinoma cells. Notably, the IWS1 rescue
140 clones used are engineered to be shRNA resistant (Sanidas et al., 2014[14]). Subsequently, we
141 confirmed the significant down-regulation of IWS1 expression after the transduction of the
142 cells with a lentiviral shIWS1 construct and the shRNA-resistant rescue of IWS1 knock-down
143 with the Flag-tagged wild type protein and phosphorylation IWS1 site mutant (**Fig. 1A**). In the
144 same cells, we performed RT-PCR investigating the inclusion of *U2AF2* E2. Consistent with
145 our previous results, *U2AF2* exon 2 inclusion occurred in shControl and shIWS1/WT-R cells
146 (**Fig. 1A**) (Laliotis et al., 2020[15]).

147 To further investigate our hypothesis, we fractionated the nuclear and cytosolic
148 compartments of shControl, shIWS1, shIWS1/WT-R, shIWS1/MT-R, shIWS/U2AF65α, and
149 shIWS1/U2AF65β NCI-H522 and NCI-H1299 cell lines, and calculated the Cytoplasmic to
150 Nuclear (C/N) ratio of the set of intronless genes with qRT-PCR. Notably, in order to induce
151 the transcription of type I IFNs (*IFNA1 and IFNB1*), we infected cells with the murine
152 paramyxovirus, Sendai fused with GFP (SeV-GFP), which is a potent and commonly used tool
153 for induction of type I IFNs (Yount et al., 2006[19], Bedsaul et al., 2016[20]). First, using western
154 blotting, we confirmed the validity of the fractionation by the detection of Lamin A/C and
155 GAPDH only in the nuclear and cytosolic protein compartment, respectively (**Fig. S1A**). The
156 results showed decreased Cytosolic/Nuclear ratio in shIWS1 and shIWS1/MT-R, due to
157 nuclear retention of these mRNAs, which was rescued in the shIWS1/WT-R cells. More
158 importantly, consistent with our hypothesis, the ectopic expression of U2AF65α, but not the
159 U2AF65β, rescued the nuclear retention phenotype (**Fig. 1B**).

160 Next, we questioned whether IWS1 also affects the transcription of these intronless
161 genes. To this extent, we examined their total RNA levels using qRT-PCR in shControl,
162 shIWS1, shIWS1/WT-R, shIWS1/MT-R, shIWS1/U2AF65α and shIWS1/U2AF65β NCI-H522

163 and NCI-H1299 cells. Interestingly, we found that the total levels of type I IFN, *JUN* and *HSBP3*
164 were upregulated in the shIWS1 and shIWS1/MT-R cells. Interestingly, the levels of type I IFN,
165 but not *JUN and HSBP3*, were affected by the *U2AF2* RNA splicing pattern (**Fig. 1C**). We
166 interpret these data to suggest that the upregulation of the mRNAs of IFN genes in shIWS1
167 cells may be due to different mechanisms than the upregulation of the mRNAs of other
168 intronless genes. To expand the significance of these observations in human lung
169 adenocarcinoma, analysis of the publicly available data of The Cancer Genome Atlas (TCGA),
170 revealed a negative correlation of *IWS1* levels with the total RNA levels of intronless genes in
171 patients with Lung adenocarcinoma (**Fig. S1B, left panel**). Notably, consistent with the *in vitro*
172 results, analysis of the Reverse Phase Protein Assay (RPPA) in the same patients, revealed
173 a significant positive correlation of p-c-Jun (S73) with p-AKT (S473) levels and the *IWS1* and
174 *AKT3* RNA levels (**Fig. S1B**), further supporting the role of IWS1 in the nucleocytoplasmic
175 export of RNAs transcribed from intronless genes, in human lung adenocarcinoma.

176 Given that only exported mRNAs are translated into protein products, we then
177 examined the protein expression of c-Jun, Hsp27, and IFNβ1 with Western blotting in NCI-
178 H522 and NCI-H1299 cells. Similarly, SeV-GFP infection was performed in order to maximize
179 the type I IFN induction. Consistent with the qRT-PCR data, the results showed reduced
180 expression of the protein products of naturally intronless genes in shIWS1 and shIWS1/MT-R
181 cells, compared to shControl cells, an effect rescued in shIWS1/WT-R. More importantly, the
182 U2AF65α isoform rescues the shIWS1 phenotype, but the U2AF65β did not (**Fig. 1D**). These
183 data support the hypothesis that IWS1 phosphorylation controls the nucleocytoplasmic RNA
184 export transcribed from naturally intronless genes, through a process that depends on *U2AF2*
185 alternative RNA splicing.

186

187 To provide additional support to our model, protein interaction analysis using the
188 STRING database (Szklarczyk et al., 2019[21]) showed the expected interaction of U2AF65 and
189 Prp19 with components of the TREX complex and export machinery, THOC2 and Ref/Aly (**Fig.**

190 **S1C**). Furthermore, analysis of the previously performed RNA-Seq study in NCI-H522
191 shControl, shIWS1, shIWS1/WT-R, and shIWS1/MT-R cells, (Laliotis et al., 2020[15]), using
192 Gene Set Enrichment Analysis (GSEA) (Subramanian et al., 2005[21]), revealed significant
193 enrichment of genes affecting nuclear export in cells expressing phosphorylated IWS1 (**Figure**
194 **S1D**). Taken together, these results support a multi-layered role of IWS1 phosphorylation in
195 the nuclear export machinery.

196 **AKT3 kinase affects the nucleocytoplasmic export of intronless RNAs, through IWS1**
197 **phosphorylation.**

198 IWS1 is phosphorylated by AKT3, and to a lesser extent by AKT1, at Ser720/Thr721
199 (Sanidas et al., 2014[14]). The preceding data show that IWS1 phosphorylation is required for
200 the nucleocytoplasmic export of RNAs transcribed from a set of intronless genes. This raised
201 the question of whether AKT, which phosphorylates IWS1 on Ser720/Thr721, is required for
202 the activation of the pathway. To address that, we treated NCI-H522 and NCI-H1299 cells with
203 5 μM of the pan-AKT inhibitor MK2206, a dose that fully inhibits all AKT isoforms (Sanidas et
204 al., 2014[14], Laliotis et al., 2020[15]). The results confirmed that MK2206 inhibits AKT (S473) and
205 IWS1 phosphorylation (S720) along with the *U2AF2* exon 2 inclusion, as expected (**Fig. 2A**).
206 Following proper fractionation of these cells upon treatment with MK2206 (**Fig. S2A**), we
207 examined the C/N ratio of *IFNA1, IFNB1* (induced by SeV-GFP infection), *JUN* and *HSBP3*
208 RNA with qPCR and their protein expression. The results confirmed that inhibition of AKT
209 kinase phenocopies the loss of phosphorylated IWS1 resulting in nuclear retention of
210 intronless RNAs and subsequent downregulation of their protein products in both NCI-H522
211 and NCI-H1299 cell lines (**Fig. 2B, 2C**). To determine whether it is the AKT3 isoform, which is
212 responsible for the observed effects of AKT inhibition, we transducted NCI-H522 and NCI-
213 H1299 cells with lentiviral shAKT3 construct, along with shControl (**Fig. 2D**) and we examined
214 its effects on the nucleocytoplasmic export and expression of the same set of RNAs, following

215 successful compartment fractionation (**Fig. S2B**). The results phenocopied the inhibition with
216 MK2206 (**Fig. 2E, 2F)**, providing evidence that the observed regulation of nucleocytoplasmic
217 export depends on the phosphorylation of IWS1 by AKT3, through *U2AF2* RNA splicing.

218 **IWS1 phosphorylation is required for the proper function of the Cytoplasmic**
219 **Accumulation Region Elements (CAR-E).**

220 It has been previously reported that the consensus of Cytoplasmic Accumulation
221 Region Element (CAR-E) functions by promoting the cytoplasmic accumulation of mRNAs and
222 the production of proteins (Lei et al., 2013[13]). To further study the role of IWS1 phosphorylation
223 in the function of the CAR-E, we used a previously described construct, in which 16 tandem
224 copies of the most conserved CAR-E (CCAGTTCCTG element of *JUN*) or its mutated version
225 (CAR-E_{mut}), were inserted upstream of β-globin cDNA (**Fig. 3A**) (Lei et al., 2013[13]). As controls,
226 pCMV promoter-driven constructs encoding β-globin cDNA alone or β-globin gene containing
227 its two natural introns were analyzed in parallel. Based on previous work, the β-globin gene
228 mRNA, efficiently accumulates in the cytoplasm, whereas the β-globin cDNA transcript, is
229 normally degraded in the nucleus (Dias et al., 2010[23], Lei et al., 2011[24], Valencia et al., 2008[25]).
230 Transient transfection of these constructs in shControl, shIWS1, shIWS1/WT-R,
231 shIWS1/MT-R, shIWS1/U2AF65α, and shIWS1/U2AF65β NCI-H522 and NCI-H1299 cells
232 (**Fig. 3B, S3A**), showed proper expression of the HA-β-globin gene in all conditions,
233 independent of IWS1 phosphorylation. Furthermore, consistent with previous reports, β-globin
234 cDNAs containing the inserted mutated CAR-E element (CAR-E_{mut}), employed a similar
235 nucleocytoplasmic accumulation to the β-globin cDNA transcripts alone, with limited protein
236 expression of β-globin detected in all conditions, due to nuclear retention. In addition, the
237 insertion of 16 tandem CAR-E was efficient to induce the expression of HA-β-globin in
238 shControl cells. Strikingly, the same construct was unable to promote the expression of CAR-
239 E HA-β-globin in shIWS1 and shIWS1/MT-R cells, a phenotype rescued in shIWS1/WT-R
240 cells. More importantly, the observed shIWS1 CAR-E HA-β-globin nuclear retention

241 phenotype was rescued by U2AF65α, but not U2AF65β. These results suggest that IWS1
242 phosphorylation is required for the maintenance of CAR-E function, through *U2AF2* RNA
243 splicing.

244 **The splicing of the *U2AF2* mRNA downstream of IWS1 phosphorylation regulates the**
245 **Prp19 recruitment on the CAR-E.**

246 Based on our previous data, IWS1 phosphorylation is required for the function of the
247 CAR-E (**Fig. 3**). As mentioned above, it has been previously demonstrated that U2AF65 and
248 Prp19 affect the nucleocytoplasmic export of naturally intronless RNAs, by binding to the CAR-
249 E (Lei et al., 2013[13]). Given that aberrant splicing of *U2AF2* in shIWS1 and shIWS1/MT-R cells
250 resulted in the loss of the interaction between U2AF65 and Prp19 (Laliotis et al., 2020[15]), we
251 hypothesized that IWS1 phosphorylation affects the recruitment of the regulatory U2AF65-
252 Prp19 complex to the CAR-E elements and, eventually, their function.

253 To address this hypothesis, we performed RNA Immunoprecipitation (RIP) assays in
254 shControl, shIWS1, shIWS1/WT-R, shIWS1/MT-R, shIWS1/U2AF65α and shIWS1/U2AF65β
255 NCI-H522 and NCI-H1299 cells, using a set of primers specifically amplifying the CAR-E or
256 control regions on *IFNA1, IFNB1, JUN and HSPB3* mRNAs (**Fig. S4A**). The results confirmed
257 that both spliced variants of U2AF65 bind equally well with the CAR-E, but not the control
258 sequences (**Fig. 4A, 4B upper panels**). However, Prp19 binding to the same CAR-E regions
259 was significantly impaired in shIWS1 and shIWS1/MT-R cells, which predominantly express
260 the U2AF65β isoform (**Fig. 4A lower panels**). More importantly, the impaired Prp19 binding
261 on the CAR-E was rescued by U2AF65α, but not U2AF65β (**Fig. 4B lower panels**). These
262 results suggest that IWS1 phosphorylation controls the nucleocytoplasmic export of RNAs
263 transcribed from intronless genes, by the regulation of the U2AF65-Prp19 interaction, through
264 *U2AF2* alternative RNA splicing.

265 To further investigate the activity of this pathway in Lung Adenocarcinoma patients
266 (LUAD), we used 3 high and 3 low p-IWS1 LUAD patients, as identified in our previous work

267 (Laliotis et al., 2020[15]). Western blot and RT-PCR analysis of these samples confirmed the
268 increased expression and phosphorylation of IWS1 in the high-expressing groups with parallel
269 inclusion of *U2AF2* exon 2 (**Fig. 4C upper panels**). Following successful fractionation (**Fig.**
270 **S4B**), qRT-PCR showed decreased Cytosolic/Nuclear ratio in the low p-IWS1 group, due to
271 nuclear retention of intronless mRNAs (**Fig. 4C lower panel**). More importantly, consistently
272 with the *in vitro* data, RIP experiments in the same tumor samples revealed increased binding
273 of U2AF65 on the CAR-E in both patient groups, independent of its splicing pattern, with
274 decreased recruitment of Prp19 on the CAR-E mRNA areas in the low p-IWS1 group, which
275 predominantly express the U2AF65β (**Fig. 4D**). These data suggest that the epigenetic
276 complexes that are controlled by IWS1 phosphorylation and regulate the RNA export of
277 intronless genes, are active in Lung Adenocarcinoma patients.

278 **RNA-Pol II affects the splicing-independent nuclear export of intronless genes.**

279 Based on previous reports, U2AF65 binds RNA Pol II, leading to an U2AF65-
280 dependent recruitment of Prp19 to the newly-synthesized pre-mRNA and promoting proper
281 co-transcriptional splicing activation (C.J David et. al., 2011[26]). In order to address the possible
282 involvement of RNA Pol II in the splicing-independent RNA export, we cloned *IFNA1* and
283 *IFNB1* cDNAs in the lentiviral vectors pLx304 and pLKO.1, which drive their expression
284 through CMV (RNA Pol II-dependent) and U6 (RNA Pol III-dependent) promoters, respectively
285 (**Fig. S5A**) (Schramm et al., 2002[27]). We then transduced NCI-H522 and NCI-H1299 cells with
286 lentiviral shIFNα1 or shIFNβ1, in order to remove the endogenous mRNA products.
287 Subsequently, we rescued their expression with the RNA Pol II (pLx304-R) or RNA Pol III-
288 driven (pLKO.1-R) lentiviral construct and addressed the expression of *IFNA1* or *IFNB1* with
289 qRT-PCR, following SeV-GFP infection. The results confirmed the significant downregulation
290 of *IFNA1* and *IFNB1* expression in the shIFNα and shIFNβ cells, respectively, with robust
291 expression in both pLx304-R and pLKO.1-R cells. (**Fig. 5A left panel**). To further investigate
292 the role of RNA Pol II in the nucleocytoplasmic export of type I IFNs, we fractionated the same
293 NCI-H522 and NCI-H1299 cells (**Fig. S5B**) and measured the C/N ratio with qRT-PCR,

294 following SeV-GFP infection. Interestingly, the results showed nuclear retention and
295 downregulation of IFNβ1 levels in the pLKO.1-R cells, an effect rescued in pLx304-R cells.
296 (**Fig. 5A right panels, 5B**). These results suggest that RNA Pol II is involved in the regulation
297 of the splicing-independent RNA export of naturally intronless RNAs.

298 **The loss of IWS1 phosphorylation enhances viral infection through the aberrant p-**
299 **STAT1 signaling and transcription of ISGs.**

300 The preceding data suggest that IWS1 phosphorylation affects the nucleocytoplasmic
301 export and expression of type I IFNs, through the regulation of the U2AF65-Prp19 interaction
302 and their recruitment to CAR-E elements of *IFNA1 and IFNB1* mRNAs. Given that type I IFNs
303 orchestrate the cellular antiviral response (Lazear et al., 2019[28]), we hypothesized that loss of
304 IWS1 phosphorylation will accordingly increase viral replication, due to the downregulation of
305 type I IFNs. To this extent, we infected NCI-H522 and NCI-H1299 shCon, shIWS1,
306 shIWS1/WT-R and shIWS1/MT-R cells with a set of viral strains including Vesicular Stomatitis
307 Virus (VSV-GFP), Sendai (SeV-GFP), Reovirus and Influenza A virus (IAV-GFP) and we
308 monitored the levels of infections with flow cytometry (Chesarino et al., 2015[29], Kenney et al.,
309 2019[30], Sermersheim et al., 2020[31]). To carry out these experiments we used short hairpin
310 RNA constructs in a pGIPZ vector we modified by deleting the GFP cassette. Consistently,
311 the results showed increased infection by all viral strains in shIWS1 and shIWS1/MT-R cells,
312 a phenotype rescued in shIWS1/WT-R cells, which parallels the nucleocytoplasmic distribution
313 and reduced expression of type I IFNs. (**Fig. 6A, S6A**).

314 Based on the latter data, we then questioned whether the observed downregulation of
315 type I IFNs upon the loss of phosphorylated IWS1 affects the IFN downstream signaling
316 pathways and the induction of Interferon Stimulated Genes (ISGs). To address this question,
317 we infected NCI-H522 shControl and shIWS1 cells with VSV-GFP virus. After 16h of infection,
318 the cells were harvested for RNA and the supernatant derived from each condition was used
319 to stimulate NCI-H522 parental cells, for various time intervals (**Fig. 5B**). Western blot analysis
320 of protein extracts from these intervals, revealed robust activation of p-STAT1 (Y701) after the

321 stimulation of NCI-H522 cells with shControl-derived supernatant, with a parallel expression
322 of IFNβ1, phenomenon not triggered by the stimulation with the shIWS1-derived supernatant
323 (**Fig. 5C, upper panel**).

324 The increase in the abundance of IFNβ1, within 10 minutes from the start of the
325 stimulation, was surprising because it was too rapid to be due by the induction of the *IFNB1*
326 gene. Previous studies had shown that IFNβ1 undergoes endocytosis and that it can be siloed
327 in endosomes, where it can be detected for days following IFN treatment (Altman et al.,
328 2020[32]). Based on this information, we hypothesized that IFNβ1 detected in this experiment
329 was endocytosed from the supernatants of shControl cells. To address this hypothesis we
330 treated parental NCI-H522 cells with recombinant human IFNβ1 and we probed the cell lysates
331 harvested at sequential time points with antibodies to IFNβ1. The results confirmed the rapid
332 accumulation of the recombinant IFNβ1 in the harvested cell lysates (**Fig. S6B**).

333 To further support our data, and given that p-STAT1 is a main component of the
334 Interferon Stimulated Gene Factor 3 (ISGF3) for the transcriptional induction of ISGs (Wang
335 et al., 2017[33]), we performed Chromatin Immuno Cleavage (ChIC) assays in NCI-H522 cells
336 stimulated for 30' with shControl or shIWS1-derived supernatant, along with unstimulated
337 cells. Consistent with the p-STAT1 activation pattern, the results showed increased binding of
338 p-STAT1 (Y701) to the Interferon Stimulated Response Elements (ISREs) of the major ISGs
339 *IRF1, IRF9, STAT1,* and *STAT2*, in the shControl-derived stimulated cells (**Fig. 6C, lower**
340 **panel**). Notably, total RNA extracted from NCI-H522 shControl, shIWS1, shIWS1/WT-R, and
341 shIWS1/MT-R cells following VSV-GFP infection, revealed robust downregulation of a set of
342 20 ISGs in shIWS1 and shIWS1/MT-R cells, a phenotype rescued in shIWS1/WT-R cells (**Fig.**
343 **6D**). More importantly, the treatment of NCI-H522 cells with the clinically used pan-AKT
344 inhibitor MK2206 followed by VSV-GFP infection phenocopied the ISGs signature
345 downregulation upon loss of IWS1 phosphorylation (**Fig. 6E**) and parallels the expression of
346 type IFNs and p-STAT1 activation. Altogether, these data suggest that IWS1 phosphorylation
347 by AKT kinase, regulates viral replication, through the nucleocytoplasmic export of type I IFNs
348 and the subsequent activation of p-STAT1 and induction of ISGs.

349 **Inhibition of the AKT/p-IWS1 axis sensitizes lung adenocarcinoma cells to oncolytic**
350 **viral killing.**

351 Based on the preceding data, loss of IWS1 phosphorylation enhances viral replication
352 by affecting the induction of p-STAT1 and ISGs, due to impaired type I IFNs expression. We
353 then hypothesized that IWS1 would affect the sensitivity of lung adenocarcinoma cells to
354 oncolytic viral infection, through the regulation of type I IFN response. To determine whether
355 IWS1 phosphorylation affects the sensitivity of lung adenocarcinoma cells to infection with
356 oncolytic viruses, we used the viral strains VSV-GFP and Reovirus, which are widely tested
357 as potential virotherapy in a variety of solid tumors, including lung cancer (Schreiber et al.,
358 2019[34], Villalona-Calero et al., 2016[35]). By infecting NCI-H522 and NCI-H1299 shControl,
359 shIWS1, shIWS1/WT-R, and shIWS1/MT-R cells with increasing Multiplicity of Infection (MOI),
360 we observed increased viral-induced killing of shIWS1 and shIWS1/MT-R cells by VSV and
361 Reovirus, after 16h and 48h of infection respectively, compared to shControl and shIWS1/WT-
362 R cells (**Fig. 7A, S7A**). It is worth mentioning that according to our previous observations, the
363 NCI-H522 and NCI-H1299 shIWS1 cells do not exhibit proliferation deficits upon 48h,
364 compared to the shControl cells, suggesting that the observed effect is solely due to the viral
365 infection (Laliotis et al., 2020[15]). More importantly, the treatment of NCI-H522 and NCI-H1299
366 cells with the pan-AKT inhibitor MK2206, sensitized the cancer cells to viral killing by VSV and
367 Reovirus, phenocopying the loss of IWS1 phosphorylation (**Fig. 7B, S7B**).

368 To further demonstrate the cellular events following the infection with the oncolytic
369 viruses, NCI-H522 and NCI-H1299 shControl and shIWS1 cells were infected with VSV
370 (MOI=1) for several time point intervals, and cleavage of PARP, a hallmark of Caspase-
371 mediated death, was examined by Western Blotting (Chaitanya et al., 2010[36]). Strikingly, the
372 results revealed robust PARP-cleavage in the shIWS1 cells, observed at the early time points
373 compared to the shControl cells, further supporting our hypothesis (**Fig. 7C, S7C**). These data
374 come in agreement with the effect of IWS1 phosphorylation on the nucleocytoplasmic

375 distribution of type I IFNs (**Fig. 1, Fig. 2**), the function of the CAR-E elements (**Fig. 3, Fig 4**),
376 the pattern of viral infection and the activation of p-STAT1 and the downstream ISGs (**Fig. 5**).
377 Altogether, these data confirm our model in which, IWS1 phosphorylation by AKT
378 kinase at S720/T721 controls the epigenetic regulation of *U2AF2* alternative RNA splicing,
379 leading to the inclusion of exon 2. The exon 2-containing U2AF65α isoform binds and recruits
380 Prp19 on the CAR-E of *IFNA1* and *IFNB1*, promoting their nucleocytoplasmic export. During
381 oncolytic viral infection, the latter facilitates proper type I IFN expression, activation of the p-
382 STAT1/ISGF3, and transcription of ISGs, enhancing the resistance of lung adenocarcinoma
383 cells to oncolytic viral infection (**Fig. 8**)

384 **Discussion**

385 Our results implicate IWS1 phosphorylation as a regulator of the nucleocytoplasmic
386 export of naturally intronless RNAs and the type I IFN response. We report a pathway initiated
387 by the AKT3-mediated phosphorylation of IWS1 (**Fig. 1, Fig. 2**), which induces the alternative
388 RNA splicing of *U2AF2* (Laliotis et al., 2020[37]). This shift in the alternative RNA splicing pattern
389 controls the interaction of U2AF65 with yet another splicing factor, Prp19. These two factors
390 interact and regulate the nucleocytoplasmic export and expression of naturally intronless
391 genes *IFNA1, IFNB1, JUN* and *HSPB3,* by affecting the function of CAR-E and directly binding
392 on these elements (**Fig. 3, Fig. 4**). Subsequently, our findings suggest that inhibition of this
393 pathway enhances viral replication in the infected cells, due to the downregulation of type I
394 IFNs. Notably, this effect on viral replication is mediated by aberrant activation of p-STAT1
395 signals and active transcription of ISGs (**Fig. 6**). Finally, this manipulation of type I IFNs
396 response through the inhibition of the AKT/p-IWS1 axis sensitizes lung adenocarcinoma cells
397 to oncolytic viral killing mediated by Caspase signals (**Fig. 7**).
398 An important conclusion, based on the data presented in this report, is that the
399 epigenetic regulation of alternative RNA splicing, through IWS1 phosphorylation, along with

400 the downstream effect on splicing machinery, affects the splicing-independent nuclear export
401 of naturally intronless mRNAs. AKT kinase-mediated signals, through IWS1 phosphorylation,
402 affect *U2AF2* alternative RNA splicing and the U2AF65-Prp19 interaction and their function on
403 the splicing-independent export. This is also supported by previous work showing that splicing
404 factors are also associated with CAR-E (Lei et al., 2013[13]) and that many of them interact with
405 adapter proteins of the export machinery (Müller-McNicoll et al., 2016[38]). These data provide
406 insight into the explanation that splicing factors provide the backbone for protein-protein
407 interactions with export machinery components, inducing the export of these genes. In
408 addition, we provide evidence that IWS1 phosphorylation is necessary for the function of the
409 CAR-E (**Fig. 3**). Given that these elements have been identified in the majority of intronless
410 genes (Lei et al., 2011[24], Valencia et al., 2008[25], Lei et al., 2013[13]), our data suggest a global
411 role of the AKT/p-IWS1 axis in the regulation of splicing-independent export, through *U2AF2*
412 RNA splicing.

413 Interestingly, although IWS1 phosphorylation affects the export of intronless genes,
414 our results also show a negative correlation of IWS1 with their RNA expression in cell lines
415 and LUAD patients (**Fig. 1**). Notably, the *U2AF2* RNA splicing pattern affects the expression
416 of type IFNs mRNA, but not the one of *JUN* and *HSBP3*. Based on our recent data, loss of
417 IWS1 phosphorylation promotes genomic instability, through a process dependent on *U2AF2*
418 RNA splicing, leading to cytosolic DNA and transcription upregulation of type IFNs (Laliotis et
419 al., 2020[39]). The exact role of this pathway in the transcriptional regulation of these genes will
420 be addressed in future studies.

421 Our data also indicate that RNA Pol II contributes to the regulation of the nuclear export
422 of intronless RNAs (**Fig. 5**). Nonetheless, components of the TREX complex have been shown
423 to be efficiently loaded onto mRNAs even in the absence of splicing and regulate this process
424 (Akef et al., 2015[40], Lee, E.S. et al., 2015[41], Lee, E.S. et al., 2020[42]). Given that the TREX
425 complex is recruited to target genes by RNA Pol II co-transcriptionally (Sträßer et al., 2002[43]),
426 this suggests that the observed effect of RNA Pol II in this process may be through the

427 recruitment of TREX complex on these intronless genes. The exact role of RNA Pol II in this
428 process will be elucidated in future studies.

429 In the present study, we also demonstrated that signals originating from AKT3 kinase
430 regulate viral replication due to the regulation of type I IFNs, through IWS1 phosphorylation.
431 Specifically, suppression of the AKT3/p-IWS1 axis disrupts the U2AF65-Prp19 interaction,
432 leading to nuclear retention and downregulation of type IFNs (**Fig. 1, Fig. 2**). The latter
433 enhances viral replication of a set of viral strains, due to impaired ISGs induction (**Fig. 6**). The
434 PI3K/Akt pathway appears to be associated with the host cell immune response to counteract
435 viral infection, in an isoform-specific manner (Diehl et al., 2013[44]). Based on our previous work,
436 AKT1 selectively phosphorylates EMSY and stimulates the expression of ISGs (Ezell et al.,
437 2012[11]). In the present work, we demonstrate the opposing role of the AKT3 isoform in the
438 expression of ISG, through IWS1 phosphorylation. The fact that the selective inhibition of
439 some of these pathways, such as the EMSY or the IWS1 pathway, had profound effects on
440 the sensitivity of the cells to viral infection, suggests that these pathways may not function
441 independently of each other and that their roles may not be additive, but synergistic. A recent
442 report, consistent with our findings, found that PI3K/AKT blockade enhances the replication of
443 Reovirus by repressing ISGs (Tian et al., 2015[45]). Importantly, our data also implicate that
444 alternative RNA splicing and RNA processing can regulate the immune and type I IFN
445 response during viral infection. Given the fact that aberrant splicing is known to contribute to
446 defects in IFN response and viral replication (Chauhan et al., 2019[46], Chang et al., 2017[47]),
447 our data support another layer of this regulation through RNA export and processing.

448 Our findings support that inhibition of the AKT/p-IWS1 axis sensitizes the cells to
449 oncolytic viral killing, through the manipulation of RNA processing and export. These results
450 come in agreement with previous reports supporting that PI3K/AKT inhibition sensitizes cancer
451 cells to oncolytic viral infection (Tong et al., 2015[48]). Interestingly, in the case of non-small cell
452 lung cancer (NSCLC), several reports have demonstrated the synergistic role of Reovirus and
453 VSV oncolytic viruses to the clinical outcome of lung cancer patients (Villalona-Calero et al.,
454 2016[35], Bishnoi et al., 2018[49]), with several ongoing clinical trials to date (NCT03029871,

455 NCT00861627). Notably, a preclinical *in vivo* lung cancer model with genetic ablation of
456 *IFNAR1* (*IFNAR1*$^{-/-}$*),* demonstrates synergistic therapeutic effects of VSV (Schreiber et al.,
457 2019[34]). Our data reveal that inhibition of the AKT/p-IWS1 axis downregulates the induction of
458 ISGs following VSV infection, including *IFNAR1* (**Fig. 6**), further supporting the role of the
459 AKT/IWS1 axis to the response to oncolytic viruses.

460 Another important clinical application of this pathway is that OVs often induce IFN
461 release in the Tumor Microenvironment (TME), resulting in an upregulation of PD-L1
462 expression on tumor cells (Bellucci et al., 2015[50]). Previous studies have shown that the
463 combination of Reovirus with PD-1 blockade enhanced the ability of NK cells to kill reovirus-
464 infected tumor cells, increased CD8+T cells, and enhanced the antitumor immune response
465 (Rajani et al., 2016[51]). Further studies proposed that a triple combination of anti–CTLA-4, anti–
466 PD-1, and oHSV–IL-12 resulted in long-term durable cures in most of the mice treated in two
467 syngeneic models of GBM by inducing a profound increase in the ratio of T effector to Tregs
468 (Saha et al., 2017[52]). More importantly, oncolytic viruses preferentially replicate in tumour cells
469 because the antiviral responses in these cells are dysfunctional (Xia et al., 2016[53]). In healthy
470 tissue, the production of interferons and interferon-related factors limits viral replication and
471 boosts the rate of viral clearance, suggesting limited potential side effects (Bommareddy et
472 al., 2018[54]). Driven by these strong evidences of the synergistic effect of OV with immune-
473 checkpoint inhibitors, several clinical trials have actively investigated the possible synergy
474 between these therapeutic approaches, with promising results (NCT02263508,
475 NCT02307149, NCT03153085).

476 The data in this report may also be relevant for the design of strategies to prevent or
477 overcome the resistance of *EGFR* mutant lung adenocarcinomas to Tyrosine kinase Inhibitors
478 (TKI). Our recent studies had shown that the IWS1 phosphorylation pathway is active in
479 human lung adenocarcinoma. More importantly, IWS1 phosphorylation and *U2AF2* exon 2
480 inclusion were shown to correlate positively with tumor stage, histologic grade and metastasis,
481 and to predict poor survival in patients with *EGFR* mutant, but not *KRAS* mutant tumors
482 (Laliotis et. al 2020[15]). A recent publication provided evidence, linking resistance to EGFR

483 inhibitors to the upregulation of type I IFN signaling (Gong et al., 2020[55]). This suggests that
484 by promoting type I IFN signaling, the IWS1 phosphorylation pathway may promote resistance
485 to EGFR TKI, contributing to the poor prognosis of these tumors.

486 Our data also show that the U2AF65/Prp19 spliceosomal complex that controls the
487 RNA export of intronless genes and recruited upon IWS1 phosphorylation, is active in Lung
488 Adenocarcinoma patients, suggesting it as a possible therapeutic target for the manipulation
489 of the IFN response in these patients. Based on the latter, we provide the rationale for three
490 potential translation applications. First, the combination of AKT/IWS1 inhibitors with oncolytic
491 viruses may enhance their lytic action in lung adenocarcinoma due to the suppression of the
492 induction of ISGs. Second, IWS1 inhibition could enhance the response of lung
493 adenocarcinoma patients treated with OV/PD-1 inhibitors, or the p-IWS1 levels may act as
494 precision medicine marker for response to OV or the OV/PD-1 blockade combination, through
495 the regulation of IFN response in the TME. Third, given that the IWS1 phosphorylation-
496 dependent effect on the response to oncolytic viruses is mediated through manipulation of
497 RNA splicing and RNA processing and a specific *U2AF2* isoform, a process occurring in LUAD
498 patients as well (**Fig. 4**), the oncolytic efficiency in lung adenocarcinoma patients may be
499 enhanced with the use of highly isoform-specific antisense oligonucleotides and
500 pharmacologic modulators of splicing machinery (Obeng et al., 2019[56]), which are currently
501 under clinical trials (NCT03901469, NCT02711956, NCT02268552, NCT02908685).

502 Collectively, our results describe a novel pathway through IWS1 phosphorylation by
503 AKT which, through the regulation of RNA processing and export machinery, may serve as a
504 precision-medicine marker for response and important synergy target for the therapeutic
505 outcome of oncolytic viral therapy in lung adenocarcinoma.

506

507 **Materials and Methods**

508 **Cells and culture conditions, transfections and inhibitors**

509 Cells, inhibitors and shRNAs, lentiviral constructs and experimental protocols are described in
510 detail in the supplemental experimental procedures. Experimental protocols include use of
511 inhibitors, transient transfections, lentiviral packaging, and cellular transduction with lentiviral
512 constructs.

513 **Expression Vectors and shRNAs**

514 The origin of the expression clones and shRNAs are described in Supplementary Table S3.
515 The cloning of *IFNA1* and *IFNB1* cDNA in the pLx304-V5 and pLKO.1 vectors is described in
516 the Supplementary Experimental Procedures. The pGIPZ shIWS1 clone used in this report
517 (Sanidas et al., 2014[14], Laliotis et al., 2020[15]), was subjected to modification in order to remove
518 the GFP cassette, are also described in the Supplementary Experimental Procedures.

519 **Immunoblotting**

520 Cells were lysed with RIPA buffer and cell lysates were resolved by electrophoresis in SDS-
521 PAGE and analyzed by immunoblotting. Images were acquired and analyzed, using the Li-
522 Cor Fc Odyssey Imaging System (LI-COR Biosciences, Lincoln, NE). For the lists of antibodies
523 used for immunoprecipitation and western blotting and for other details, see Supplemental
524 Experimental Procedures.

525 **Subcellular Fractionation**

526 Cell pellets were fractionated into nuclear and cytoplasmic fractions, which were used to
527 measure the relative abundance of proteins and RNAs in the nucleus and the cytoplasm, as
528 described before (Laliotis et al., 2020[15]). For details, see Supplemental Experimental
529 Procedures.

530 **RT-PCR and qRT-PCR**

531 Total RNA was isolated using the PureLink RNA Kit (Invitrogen, Cat. No 12183018A). Isolated
532 RNA was analyzed by real-time RT-PCR for the expression of the indicated mRNAs. The
533 mRNA levels were normalized based on the levels of GAPDH or 18S rRNA (internal control).
534 The primer sets used are listed in the Supplemental Experimental Procedures.

535 **Chromatin Immuno-Cleavage (ChIC)**

536 The binding of p-STAT1 on ISRE of ISGs was addressed by chromatin Immuno-cleavage
537 (Skene et al., 2018[57], Laliotis et al., 2020[15]). For details, for the ChIC protocols. see
538 Supplemental Experimental Procedures.

539 **Virus propagation and titering**

540 Influenza virus A/PR/8/1934 (H1N1) expressing green fluorescent protein (PR8-GFP) was
541 propagated in 10-day-old embryonated chicken eggs (Charles River Laboratories) for 48 hours
542 at 37°C and titered in MDCK cells. Sendai virus expressing GFP (SEV-GFP) was propagated
543 in 10-day-old embryonated chicken eggs at 37°C for 40 hours and titered on Vero cells. VSV
544 expressing GFP (VSV-GFP) was propagated and titered in HeLa cells. Reovirus was
545 propagated and titered in Vero cells.
546

547 **Cell infections and flow cytometry**

548 NCI-H522 cells were infected with PR8-GFP or Reovirus at an MOI of 1.0 for 24h, or with
549 VSV-GFP or SEV-GFP at an MOI of 0.5 for 16h. NCI-H1299 cells were infected with_PR8-
550 GFP at an MOI of 1.0 for 24h, or with VSV-GFP or SEV-GFP at an MOI of 0.25 for 24h.
551 Following infection, cells were fixed in 4% paraformaldehyde (Thermo Scientific),
552 permeabilized with 0.1% Triton X-100 in PBS, and incubated with PBS containing 2% fetal
553 bovine serum. Reovirus-infected cells were stained with anti-reovirus T3D sigma 3 antibody
554 (DSHB, 10G10), followed by anti-mouse Alexa488-conjugated secondary antibody (Thermo

555 Scientific, A-11029). PR8, VSV, and SEV infection rates were measured by detecting virus-
556 encoded GFP. Flow cytometry was performed on a FACSCanto II flow cytometer (BD
557 Biosciences) and analyzed using FlowJo software (DB, Ashland, OR).

558 **RNA Immunoprecipitation**

559 The binding of RNA binding proteins to regions of the IFNα, IFNβ, c-Jun and HSPB3 mRNAs
560 was addressed by RNA Immunoprecipitation, as described before (Laliotis et al., 2020[15]). For
561 details, see Supplemental Experimental Procedures.

562 **Cellular Survival/Killing curves**

563 For the determination of cell survival following oncolytic viral infections, NCI-H522 and NC-
564 H1299 cells were plated in 24-well plates. The cells were exposed to increased MOI of VSV
565 and Reovirus for 16h and 48h, respectively. After the incubation period, cell proliferation was
566 quantified by fluorescent detection of the reduction of resazurin to resorufin by viable cells and
567 normalized to DMSO-treated wells, using alamarBlue™ HS Cell Viability Reagent (Thermo
568 Fisher Cat. No A50100), as described in the Supplemental Experimental Procedures.

569 **TCGA/RPPA analysis**

570 TCGA data were downloaded from https://portal.gdc.cancer.gov/ and analysed as described
571 in the Supplemental Experimental Procedures.

572 **Data availability**

573 All the source data derived from this report have been deposited in the Mendeley Dataset.
574 (Laliotis et al., 2020[58], doi: 10.17632/853gfbbx7m.1)

575 **Statistical analysis**

576 All the statistical analysis was performed in GraphPad Prism, as described in the
577 corresponding section. All the statistical analysis reports can be found in the Mendeley dataset

578 where the source data of this report were deposited. (Laliotis et al., 2020[58], doi:
579 10.17632/853gfbbx7m.1)

580 **Acknowledgments**

581 The authors wish to thank all the members of the Tsichlis Lab for helpful discussions. We also
582 thank Dr Samir Achaya for reviewing the manuscript before the submission. This work was
583 supported by the NIH grant R01 CA186729 to P.N.T., the NIH grant R01 CA198117 to P.N.T
584 and V.C, by start-up funds from the OSUCCC to P.N.T,, from the National Center for
585 Advancing Translational Sciences grant KL2TR002734 to L.S. G.I.L is supported by the
586 Pelotonia Post-Doctoral fellowship from OSUCCC.

587 **Author Contributions**

588 **G.I.L.** Conceptualization, overall experimental design. Performed all the experiments except
589 the viral infections in Figure 6, analyzed the data, prepared the figures and wrote the
590 manuscript. **A.D.K.** Designed and performed all the infections with viral strains, optimized,
591 performed and analyzed the flow cytometry experiments and edited the manuscript **E.C.**
592 Designed and performed with G.I.L the time point interval experiment for p-STAT1 activation
593 and Caspase-mediated death in Figure 6 and Figure 7, edited the manuscript **A.O.** Assisted
594 to the time point interval experiment for Caspase-mediated death and edited the manuscript
595 **A.K.K** Performed the cloning of the type I IFN vectors for RNA Pol II and III promoter
596 expression, performed RT-PCR experiments **A.L.F.** Bioinformatics analyses of RNA-Seq and
597 TCGA data, edited the manuscript. **V.A.** Assisted to the time point interval experiment for p-
598 STAT1 activation and edited the manuscript **J.D.B** Advised on the design of experiments and
599 edited the manuscript **C.T.** Advised on the design of experiments and edited the manuscript.
600 **L.S.** Advised on the design of experiments and edited the manuscript **V.C.** Contributed to
601 overall experimental design, edited the manuscript. **J.S.Y** Designed the viral infection
602 experiments and contributed to overall experimental design, edited the manuscript **P.N.T.**
603 Overall experimental design, manuscript writing and editing.

604

605 **References**

606

607 1. Frisch, S.M. and MacFawn, I.P., 2020. Type I interferons and related pathways in cell
608 senescence. *Aging Cell*, p.e13234.
609 2. Acosta, P.L., Byrne, A.B., Hijano, D.R. and Talarico, L.B., 2020. Human Type I
610 Interferon Antiviral Effects in Respiratory and Re Emerging Viral Infections. *Journal of*
611 *Immunology Research*, *2020*.
612 3. Amarante-Mendes, G.P., Adjemian, S., Branco, L.M., Zanetti, L.C., Weinlich, R. and
613 Bortoluci, K.R., 2018. Pattern recognition receptors and the host cell death molecular
614 machinery. *Frontiers in immunology*, *9*, p.2379.
615 4. Ablasser, A. and Hur, S., 2019. Regulation of cGAS-and RLR-mediated immunity to
616 nucleic acids. *Nature Immunology*, pp.1-13.
617 5. Aleynick, M., Svensson-Arvelund, J., Flowers, C.R., Marabelle, A. and Brody, J.D.,
618 2019. Pathogen molecular pattern receptor agonists: treating cancer by mimicking
619 infection. *Clinical Cancer Research*, *25*(21), pp.6283-6294.
620 6. Park, A.K., Fong, Y., Kim, S.I., Yang, J., Murad, J.P., Lu, J., Jeang, B., Chang, W.C.,
621 Chen, N.G., Thomas, S.H. and Forman, S.J., 2020. Effective combination
622 immunotherapy using oncolytic viruses to deliver CAR targets to solid tumors. *Science*
623 *Translational Medicine*, *12*(559).
624 7. Rehman, H., Silk, A.W., Kane, M.P. and Kaufman, H.L., 2016. Into the clinic:
625 Talimogene laherparepvec (T-VEC), a first-in-class intratumoral oncolytic viral therapy.
626 *Journal for immunotherapy of cancer*, *4*(1), pp.1-8.
627 8. Martinez-Quintanilla, J., Seah, I., Chua, M. and Shah, K., 2019. Oncolytic viruses:
628 overcoming translational challenges. *The Journal of Clinical Investigation*, *129*(4),
629 pp.1407-1418.

630 9. Kroczynska, B., Mehrotra, S., Arslan, A.D., Kaur, S. and Platanias, L.C., 2014.
631 Regulation of interferon-dependent mRNA translation of target genes. *Journal of*
632 *Interferon & Cytokine Research*, *34*(4), pp.289-296.
633 10. Gantner, B.N., Jin, H., Qian, F., Hay, N., He, B. and Richard, D.Y., 2012. The Akt1
634 isoform is required for optimal IFN-β transcription through direct phosphorylation of β-
635 catenin. *The Journal of Immunology*, *189*(6), pp.3104-3111.
636 11. Ezell, S.A., Polytarchou, C., Hatziapostolou, M., Guo, A., Sanidas, I., Bihani, T., Comb,
637 M.J., Sourvinos, G. and Tsichlis, P.N., 2012. The protein kinase Akt1 regulates the
638 interferon response through phosphorylation of the transcriptional repressor EMSY.
639 *Proceedings of the National Academy of Sciences*, *109*(10), pp.E613-E621.
640 12. de Padilla, C.M.L. and Niewold, T.B., 2016. The type I interferons: Basic concepts and
641 clinical relevance in immune-mediated inflammatory diseases. *Gene*, *576*(1), pp.14-
642 21.
643 13. Lei, H., Zhai, B., Yin, S., Gygi, S. and Reed, R., 2013. Evidence that a consensus
644 element found in naturally intronless mRNAs promotes mRNA export. *Nucleic acids*
645 *research*, *41*(4), pp.2517-2525.
646 14. Sanidas, I., Polytarchou, C., Hatziapostolou, M., Ezell, S.A., Kottakis, F., Hu, L., Guo,
647 A., Xie, J., Comb, M.J., Iliopoulos, D. and Tsichlis, P.N., 2014. Phosphoproteomics
648 screen reveals akt isoform-specific signals linking RNA processing to lung cancer.
649 *Molecular cell*, *53*(4), pp.577-590.
650 15. Georgios I. Laliotis, Evangelia Chavdoula, Maria D. Paraskevopoulou, Abdul D. Kaba,
651 Alessandro La Ferlita, Satishkumar Singh, Vollter Anastas, Salvatore Alaimo, Arturo
652 Orlacchio, Keith A. Nair II, Vasiliki Taraslia, Ioannis Vlachos, Marina Capece,
653 ArtemisHatzigeorgiou, Dario I. Palmieri, Christos Tsatsanis, Lalit Sehgal, David P.
654 Carbone, Vincenzo Coppola, Philip N. Tsichlis, 2020 'IWS1 phosphorylation promotes
655 cell proliferation and predicts poor prognosis in EGFR mutant lung adenocarcinoma
656 patients, through the cell cycle-regulated U2AF2 RNA
657 splicing.bioRxiv2020.07.14.195297; doi: https://doi.org/10.1101/2020.07.14.195297

658 16. Georgios I. Laliotis, Evangelia Chavdoula, Maria D. Paraskevopoulou, Vollter Anastas,
659 Ioannis Vlachos, Vasiliki Tarasslia, Artemis Hatzigeorgiou, Dario Palmieri, Abdul Kaba,
660 Marina Capece, Arturo Orlacchio, Lalit Sehgal, Vincenzo Coppola and Philip N.
661 Tsichlis, Alternative RNA splicing of U2AF2, induced by AKT3-phosphorylated IWS1,
662 promotes tumor growth, by activating a CDCA5-pERK positive feedback loop, Cancer
663 Res August 15 2020 (80) (16 Supplement) 3649; **DOI:**10.1158/1538-7445.AM2020-
664 3649
665 17. Hogg, R., McGrail, J.C. and O'Keefe, R.T., 2010. The function of the NineTeen
666 Complex (NTC) in regulating spliceosome conformations and fidelity during pre-mRNA
667 splicing.
668 18. Chanarat, S. and Sträßer, K., 2013. Splicing and beyond: the many faces of the Prp19
669 complex. *Biochimica et Biophysica Acta (BBA)-Molecular Cell Research*, *1833*(10),
670 pp.2126-2134.
671 19. Yount, J.S., Kraus, T.A., Horvath, C.M., Moran, T.M. and López, C.B., 2006. A novel
672 role for viral-defective interfering particles in enhancing dendritic cell maturation. *The*
673 *Journal of Immunology*, *177*(7), pp.4503-4513.
674 20. Bedsaul, J.R., Zaritsky, L.A. and Zoon, K.C., 2016. Type I interferon-mediated
675 induction of antiviral genes and proteins fails to protect cells from the cytopathic effects
676 of Sendai virus infection. *Journal of Interferon & Cytokine Research*, *36*(11), pp.652-
677 665.
678 21. Szklarczyk, D., Gable, A.L., Lyon, D., Junge, A., Wyder, S., Huerta-Cepas, J.,
679 Simonovic, M., Doncheva, N.T., Morris, J.H., Bork, P. and Jensen, L.J., 2019. STRING
680 v11: protein–protein association networks with increased coverage, supporting
681 functional discovery in genome-wide experimental datasets. *Nucleic acids research*,
682 *47*(D1), pp.D607-D613.
683 22. Subramanian, A., Tamayo, P., Mootha, V.K., Mukherjee, S., Ebert, B.L., Gillette, M.A.,
684 Paulovich, A., Pomeroy, S.L., Golub, T.R., Lander, E.S. and Mesirov, J.P., 2005. Gene
685 set enrichment analysis: a knowledge-based approach for interpreting genome-wide

686 expression profiles. *Proceedings of the National Academy of Sciences*, *102*(43),
687 pp.15545-15550.
688 23. Dias, A.P., Dufu, K., Lei, H. and Reed, R., 2010. A role for TREX components in the
689 release of spliced mRNA from nuclear speckle domains. *Nature communications*, *1*(1),
690 pp.1-10.
691 24. Lei, H., Dias, A.P. and Reed, R., 2011. Export and stability of naturally intronless
692 mRNAs require specific coding region sequences and the TREX mRNA export
693 complex. *Proceedings of the National Academy of Sciences*, *108*(44), pp.17985-
694 17990.
695 25. Valencia, P., Dias, A.P. and Reed, R., 2008. Splicing promotes rapid and efficient
696 mRNA export in mammalian cells. *Proceedings of the National Academy of Sciences*,
697 *105*(9), pp.3386-3391.
698 26. David, C.J., Boyne, A.R., Millhouse, S.R. and Manley, J.L., 2011. The RNA polymerase
699 II C-terminal domain promotes splicing activation through recruitment of a U2AF65–
700 Prp19 complex. *Genes & development*, *25*(9), pp.972-983.
701 27. Schramm, L. and Hernandez, N., 2002. Recruitment of RNA polymerase III to its target
702 promoters. *Genes & development*, *16*(20), pp.2593-2620.
703 28. Lazear, H.M., Schoggins, J.W. and Diamond, M.S., 2019. Shared and distinct functions
704 of type I and type III interferons. *Immunity*, *50*(4), pp.907-923.
705 29. Chesarino, N.M., McMichael, T.M. and Yount, J.S., 2015. E3 ubiquitin ligase NEDD4
706 promotes influenza virus infection by decreasing levels of the antiviral protein IFITM3.
707 *PLoS Pathog*, *11*(8), p.e1005095.
708 30. Kenney, A.D., McMichael, T.M., Imas, A., Chesarino, N.M., Zhang, L., Dorn, L.E., Wu,
709 Q., Alfaour, O., Amari, F., Chen, M. and Zani, A., 2019. IFITM3 protects the heart
710 during influenza virus infection. *Proceedings of the National Academy of Sciences*,
711 *116*(37), pp.18607-18612.
712 31. Sermersheim, M., Kenney, A.D., Lin, P.H., McMichael, T.M., Cai, C., Gumpper, K.,
713 Adesanya, T.A., Li, H., Zhou, X., Park, K.H. and Yount, J.S., 2020. MG53 suppresses

714 interferon-β and inflammation via regulation of ryanodine receptor-mediated
715 intracellular calcium signaling. *Nature communications*, *11*(1), pp.1-12.
716 32. Altman, J.B., Taft, J., Wedeking, T., Gruber, C.N., Holtmannspötter, M., Piehler, J. and
717 Bogunovic, D., 2020. Type I IFN is siloed in endosomes. *Proceedings of the National*
718 *Academy of Sciences*, *117*(30), pp.17510-17512.
719 33. Wang, W., Xu, L., Su, J., Peppelenbosch, M.P. and Pan, Q., 2017. Transcriptional
720 regulation of antiviral interferon-stimulated genes. *Trends in microbiology*, *25*(7),
721 pp.573-584.
722 34. Schreiber, L.M., Urbiola, C., Das, K., Spiesschaert, B., Kimpel, J., Heinemann, F.,
723 Stierstorfer, B., Müller, P., Petersson, M., Erlmann, P. and von Laer, D., 2019. The lytic
724 activity of VSV-GP treatment dominates the therapeutic effects in a syngeneic model
725 of lung cancer. *British journal of cancer*, *121*(8), pp.647-658.
726 35. Villalona-Calero, M.A., Lam, E., Otterson, G.A., Zhao, W., Timmons, M.,
727 Subramaniam, D., Hade, E.M., Gill, G.M., Coffey, M., Selvaggi, G. and Bertino, E.,
728 2016. Oncolytic reovirus in combination with chemotherapy in metastatic or recurrent
729 non–small cell lung cancer patients with K RAS-activated tumors. *Cancer*, *122*(6),
730 pp.875-883.
731 36. Chaitanya, G.V., Alexander, J.S. and Babu, P.P., 2010. PARP-1 cleavage fragments:
732 signatures of cell-death proteases in neurodegeneration. *Cell Communication and*
733 *Signaling*, *8*(1), p.31.
734 37. Georgios I. Laliotis, Evangelia Chavdoula, Maria D. Paraskevopoulou, Vollter Anastas,
735 Ioannis Vlachos, Vasiliki Tarasslia, Artemis Hatzigeorgiou, Dario Palmieri, Abdul Kaba,
736 Marina Capece, Arturo Orlacchio, Lalit Sehgal, Vincenzo Coppola, Philip N. Tsichlis.
737 Alternative RNA splicing of U2AF2, induced by AKT3-phosphorylated IWS1, promotes
738 tumor growth, by activating a CDCA5-pERK positive feedback loop [abstract]. In:
739 Proceedings of the Annual Meeting of the American Association for Cancer Research
740 2020; 2020 Apr 27-28 and Jun 22-24. Philadelphia (PA): AACR; Cancer Res
741 2020;80(16 Suppl):Abstract nr 3649.

742 38. Müller-McNicoll, M., Botti, V., de Jesus Domingues, A.M., Brandl, H., Schwich, O.D.,
743 Steiner, M.C., Curk, T., Poser, I., Zarnack, K. and Neugebauer, K.M., 2016. SR
744 proteins are NXF1 adaptors that link alternative RNA processing to mRNA export.
745 *Genes & development*, *30*(5), pp.553-566.
746 39. Georgios I. Laliotis, Evangelia Chavdoula, Maria D. Paraskevopoulou, Abdul Kaba,
747 Alessandro La Ferlita, Vollter Anastas, Arturo Orlacchio, Vasiliki Taraslia, Ioannis
748 Vlachos, Marina Capece, Artemis Hatzigeorgiou, Dario Palmieri, Salvatore Alaimo,
749 Christos Tsatsanis, Lalit Sehgal, David P. Carbone, Vincenzo Coppola, Philip N.
750 Tsichlis. IWS1 phosphorylation promotes tumor growth and predicts poor prognosis in
751 EGFR mutant lung adenocarcinoma patients, through the epigenetic regulation of
752 U2AF2 RNA splicing [abstract]. In: Abstracts: AACR Special Virtual Conference on
753 Epigenetics and Metabolism; October 15-16, 2020; 2020 Oct 15-16. Philadelphia (PA):
754 AACR; Cancer Res 2020;80(23 Suppl):Abstract nr PO-011.
755 40. Akef, A., Lee, E.S. and Palazzo, A.F., 2015. Splicing promotes the nuclear export of
756 β-globin mRNA by overcoming nuclear retention elements. *RNA*, *21*(11), pp.1908-
757 1920.
758 41. Lee, E.S., Akef, A., Mahadevan, K. and Palazzo, A.F., 2015. The consensus 5'splice
759 site motif inhibits mRNA nuclear export. *PLoS One*, *10*(3), p.e0122743.
760 42. Eliza S Lee, Eric J Wolf, Sean S J Ihn, Harrison W Smith, Andrew Emili, Alexander F
761 Palazzo, TPR is required for the efficient nuclear export of mRNAs and lncRNAs from
762 short and intron-poor genes, *Nucleic Acids Research*, , gkaa919
763 43. Sträßer, K., Masuda, S., Mason, P., Pfannstiel, J., Oppizzi, M., Rodriguez-Navarro, S.,
764 Rondón, A.G., Aguilera, A., Struhl, K., Reed, R. and Hurt, E., 2002. TREX is a
765 conserved complex coupling transcription with messenger RNA export. *Nature*,
766 *417*(6886), pp.304-308.
767 44. Diehl, N. and Schaal, H., 2013. Make yourself at home: viral hijacking of the PI3K/Akt
768 signaling pathway. *Viruses*, *5*(12), pp.3192-3212.

769 45. Tian, J., Zhang, X., Wu, H., Liu, C., Li, Z., Hu, X., Su, S., Wang, L.F. and Qu, L., 2015.
770 Blocking the PI3K/AKT pathway enhances mammalian reovirus replication by
771 repressing IFN-stimulated genes. *Frontiers in microbiology*, *6*, p.886.
772 46. Chauhan, K., Kalam, H., Dutt, R. and Kumar, D., 2019. RNA Splicing: A New Paradigm
773 in Host–Pathogen Interactions. *Journal of molecular biology*, *431*(8), pp.1565-1575
774 47. Chang, M.X. and Zhang, J., 2017. Alternative Pre-mRNA splicing in mammals and
775 teleost fish: an effective strategy for the regulation of immune responses against
776 pathogen infection. *International journal of molecular sciences*, *18*(7), p.1530.
777 48. Tong, Y., Zhu, W., Huang, X., You, L., Han, X., Yang, C. and Qian, W., 2014. PI3K
778 inhibitor LY294002 inhibits activation of the Akt/mTOR pathway induced by an
779 oncolytic adenovirus expressing TRAIL and sensitizes multiple myeloma cells to the
780 oncolytic virus. *Oncology reports*, *31*(4), pp.1581-1588.
781 49. Bishnoi, S., Tiwari, R., Gupta, S., Byrareddy, S.N. and Nayak, D., 2018. Oncotargeting
782 by vesicular stomatitis virus (VSV): advances in cancer therapy. *Viruses*, *10*(2), p.90.
783 50. Bellucci, R., Martin, A., Bommarito, D., Wang, K., Hansen, S.H., Freeman, G.J. and
784 Ritz, J., 2015. Interferon-γ-induced activation of JAK1 and JAK2 suppresses tumor cell
785 susceptibility to NK cells through upregulation of PD-L1 expression. *Oncoimmunology*,
786 *4*(6), p.e1008824.
787 51. Rajani, K., Parrish, C., Kottke, T., Thompson, J., Zaidi, S., Ilett, L., Shim, K.G., Diaz,
788 R.M., Pandha, H., Harrington, K. and Coffey, M., 2016. Combination therapy with
789 reovirus and anti-PD-1 blockade controls tumor growth through innate and adaptive
790 immune responses. *Molecular Therapy*, *24*(1), pp.166-174.
791 52. Saha, D., Martuza, R.L. and Rabkin, S.D., 2017. Macrophage polarization contributes
792 to glioblastoma eradication by combination immunovirotherapy and immune
793 checkpoint blockade. *Cancer cell*, *32*(2), pp.253-267.
794 53. Xia, T., Konno, H., Ahn, J. and Barber, G.N., 2016. Deregulation of STING signaling in
795 colorectal carcinoma constrains DNA damage responses and correlates with
796 tumorigenesis. *Cell reports*, *14*(2), pp.282-297.

797 54. Bommareddy, P.K., Shettigar, M. and Kaufman, H.L., 2018. Integrating oncolytic
798 viruses in combination cancer immunotherapy. *Nature Reviews Immunology*, *18*(8),
799 p.498.
800 55. Gong, K., Guo, G., Panchani, N., Bender, M.E., Gerber, D.E., Minna, J.D., Fattah, F.,
801 Gao, B., Peyton, M., Kernstine, K. and Mukherjee, B., 2020. EGFR inhibition triggers
802 an adaptive response by co-opting antiviral signaling pathways in lung cancer. *Nature*
803 *Cancer*, *1*(4), pp.394-409.
804 56. Obeng, E.A., Stewart, C. and Abdel-Wahab, O., 2019. Altered RNA Processing in
805 Cancer Pathogenesis and Therapy. *Cancer discovery*, *9*(11), pp.1493-1510.
806 57. Skene, P.J. and Henikoff, S., 2017. An efficient targeted nuclease strategy for high-
807 resolution mapping of DNA binding sites. *Elife*, *6*, p.e21856.
808 58. Laliotis, Georgios I.; Kenney, Adam D.; Chavdoula, Evangelia; Orlacchio, Arturo;
809 Kaba, Abdul; La Ferlita, Alessandro; Anastas, Vollter; Beane, Joal D.; Tsatsanis,
810 Christos; Sehgal, Lalit; Coppola, Vincenzo D.; Yount, Jacob; Tsichlis, Philip N. (2020),
811 “IWS1 phosphorylation controls nucleocytoplasmic export of type I IFNs and the
812 sensitivity to oncolytic viruses, through U2AF2 RNA splicing”, Mendeley Data, V1, doi:
813 10.17632/853gfbbx7m.1

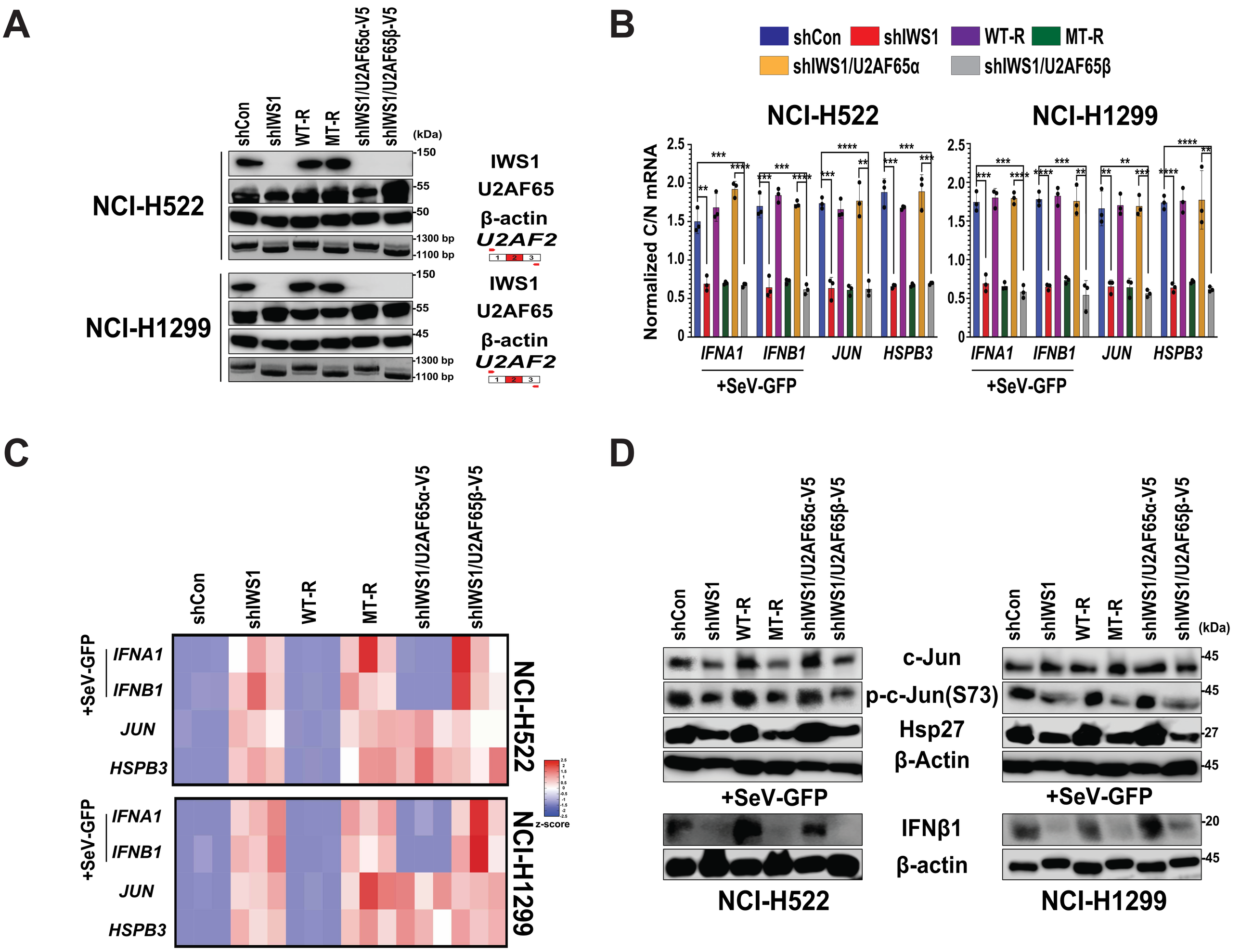
A
shCon
shIWS1
WT-R
MT-R
shIWS1/U2AF65α-V5
shIWS1/U2AF65β-V5
(kDa)
NCI-H522
NCI-H1299
IWS1
U2AF65
β-actin
U2AF2
150
55
50
45
1300 bp
1100 bp
B
shCon
shIWS1
WT-R
MT-R
shIWS1/U2AF65α
shIWS1/U2AF65β
NCI-H522
NCI-H1299
Normalized C/N mRNA
IFNA1
IFNB1
JUN
HSPB3
+SeV-GFP
C
z-score
D
c-Jun
p-c-Jun(S73)
Hsp27
β-Actin
IFNβ1
β-actin
+SeV-GFP
NCI-H522
NCI-H1299

Figure 1. IWS1 phosphorylation regulates the nucleocytoplasmic transport of mRNAs transcribed from a set of intronless genes, via *U2AF2* alternative RNA splicing.

A. Western blots of lysates of NCI-H522 and NCI-H1299 cells, transduced with the indicated constructs, were probed with anti-IWS1, anti-U2AF65 and anti-β-actin (control) antibodies. (first three lanes). RT-PCR of *U2AF2*, using oligonucleotide primers that map in exons 1 and 3 (fourth lane).

B. *IWS1 phosphorylation regulates the nucleocytoplasmic export of intronless mRNAs.* The same NCI-H522 (right panel) and NCI-H1299 (right panel) cells as in Fig. 1A, were fractionated into cytoplasmic and nuclear fractions. *IFNA1, IFNB1, JUN, HSPB3* and *GAPDH* mRNA levels in each fraction were determined using qRT–PCR. For each transcript, values are represented as cytoplasmic to nuclear ratios and were normalized to 18S rRNA. For type I IFN induction SeV-GFP infection was performed. The accuracy of the fractionation was validated with the experiment in Figure S1A. Bars show the mean normalized Cytosolic/Nuclear ratio ±SD

C. Total RNA was harvested from NCI-H522 (upper panel) and NCI-H1299 cells (lower panel), transduced with the indicated constructs. The expression of *IFNA1, IFNB1, JUN and HSPB3* mRNAs was determined by qRT-PCR and normalized to 18S rRNA. The results are represented as heatmap using z-scores from three individual biological experiments. For type I IFN induction SeV-GFP infection was performed. All assays in this figure were done in triplicate, on three biological replicates. n.s : non-significant *$p<0.05$, **$p<0.01$, ***$p<0.001$, ****$p<0.0001$. (one-side unpaired t-test).

D. Western blots of lysates of NCI-H522 (left panel) and NCI-H1299 (right panel) cells, transduced with the indicated constructs, were probed with anti-c-Jun, anti-p-c-Jun (S73), anti-Hsp27, anti-IFNβ1 and anti-β-actin (control) antibodies. For type I IFN induction SeV-GFP infection was performed. Throughout this figure NCI-H522 and NCI-H1299 cells were infected with MOI of 0.5 for 16h and MOI of 0.25 for 24h of SeV-GFP virus, respectively.

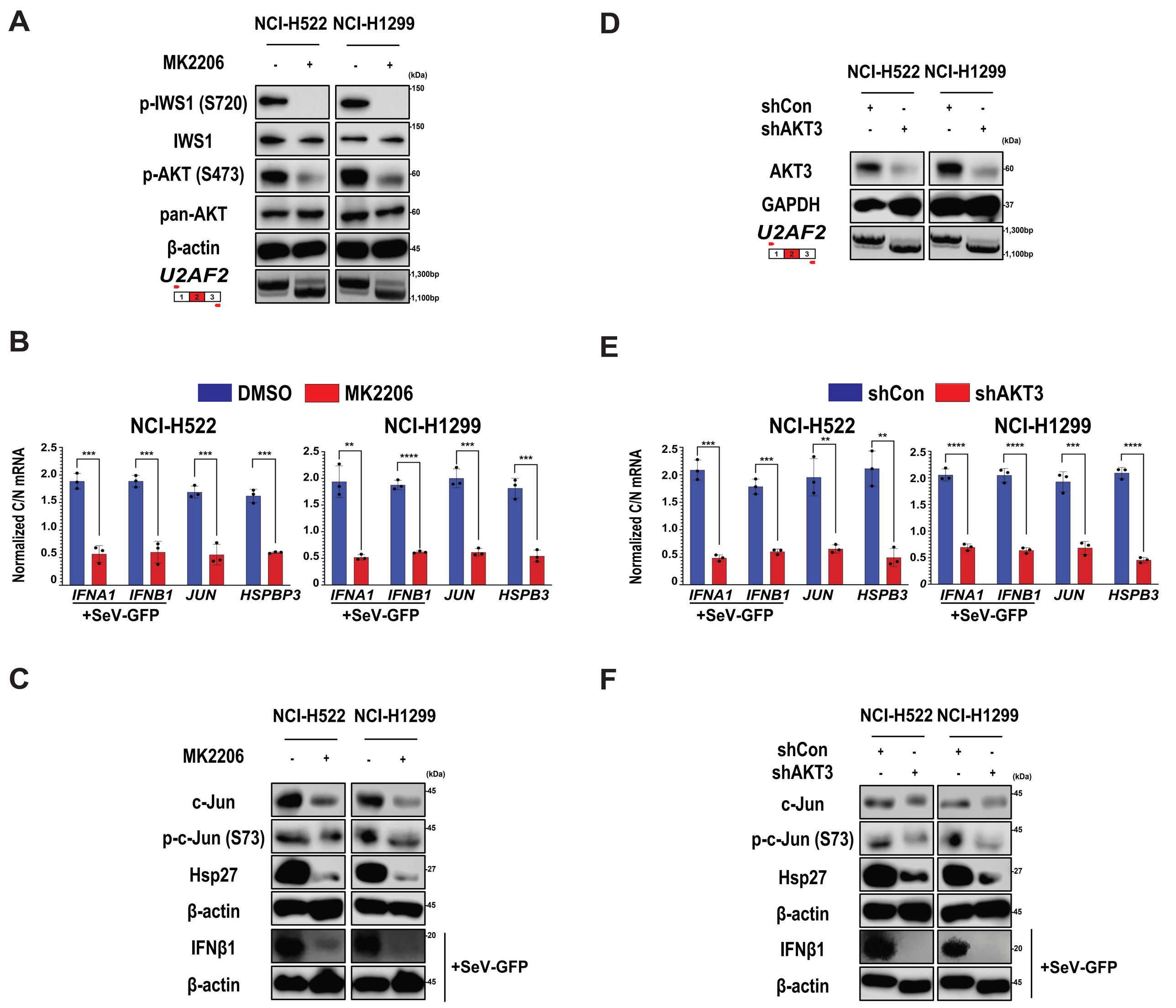
A
NCI-H522 NCI-H1299
MK2206
- + - +
(kDa)
p-IWS1 (S720)
IWS1
p-AKT (S473)
pan-AKT
β-actin
U2AF2
150
150
60
60
45
1,300bp
1,100bp
B
DMSO
MK2206
NCI-H522
NCI-H1299
Normalized C/N mRNA
IFNA1 IFNB1 JUN HSPBP3
IFNA1 IFNB1 JUN HSPB3
+SeV-GFP
C
NCI-H522 NCI-H1299
MK2206
- + - +
(kDa)
c-Jun
p-c-Jun (S73)
Hsp27
β-actin
IFNβ1
β-actin
45
45
27
45
20
45
+SeV-GFP
D
NCI-H522 NCI-H1299
shCon
shAKT3
+ - + -
- + - +
(kDa)
AKT3
GAPDH
U2AF2
60
37
1,300bp
1,100bp
E
shCon
shAKT3
NCI-H522
NCI-H1299
Normalized C/N mRNA
IFNA1 IFNB1 JUN HSPB3
IFNA1 IFNB1 JUN HSPB3
+SeV-GFP
F
NCI-H522 NCI-H1299
shCon
shAKT3
+ - + -
- + - +
(kDa)
c-Jun
p-c-Jun (S73)
Hsp27
β-actin
IFNβ1
β-actin
45
45
27
45
20
45
+SeV-GFP

Figure 2. AKT3 kinase affects the nucleocytoplasmic export of RNAs transcribed from intronless genes, thought IWS1 phosphorylation

A. NCI-H522 and NCI-H1299 cell lysates, harvested following a 4 hr treatment with MK2206 (5μM) or DMSO, were probed with the indicated antibodies. (Lower lane) RT-PCR reactions, using mRNA derived from the cells in the upper panel and oligonucleotide primers mapping in *U2AF2* exons 1 and 3 show that inhibiting Akt inhibits the inclusion of exon 2 in mature *U2AF2* mRNA transcripts in both cell lines.

B. *AKT kinase regulates the nucleocytoplasmic export of intronless mRNAs, through IWS1 phosphorylation.* Cells after similar treatment as Fig. 2A, were fractionated into cytoplasmic and nuclear fractions, *IFNα1, IFNβ1, c-Jun, HSPB3* and *GAPDH* mRNA levels in each fraction were determined using qRT–PCR. For each transcript, values are represented as cytoplasmic to nuclear ratios and were normalized to 18S rRNA. For type I IFN induction SeV-GFP infection was performed. The accuracy of the fractionation was validated with the experiment in Figure S2A. Bars show the mean normalized Cytosolic/Nuclear ratio ±SD

C. NCI-H522 and NCI-H1299 cell lysates as in Fig. 2A, were probed with the indicated antibodies. For type I IFN induction SeV-GFP infection was performed.

D. NCI-H522 and NCI-H1299 cells were transduced with lentiviral shAKT3 constructs along with shControl and their protein lysates were probed with the indicated antibodies

E. The indicated cells were fractionated into cytoplasmic and nuclear fractions, *IFNα1, IFNβ1, c-Jun, HSPB3* and *GAPDH* mRNA levels in each fraction were determined using qRT–PCR. For each transcript, values are represented as cytoplasmic to nuclear ratios and were normalized to 18S rRNA. For type I IFN induction SeV-GFP infection was performed. The accuracy of the fractionation was validated with the experiment in Figure S2B. Bars show the mean normalized Cytosolic/Nuclear ratio ±SD

F. NCI-H522 and NCI-H1299 cell lysates as in Fig. 2D, were probed with the indicated antibodies. For type IFN induction SeV-GFP infection was performed. Throughout this figure NCI-H522 and NCI-H1299 cells were infected with MOI of 0.5 for 16h and MOI of 0.25 for 24h of SeV-GFP virus, respectively. All assays in this figure were done in triplicate, on three biological replicates. n.s : non-significant *$p<0.05$, **$p<0.01$, ***$p<0.001$, ****$p<0.0001$. (one-side unpaired t-test).

A

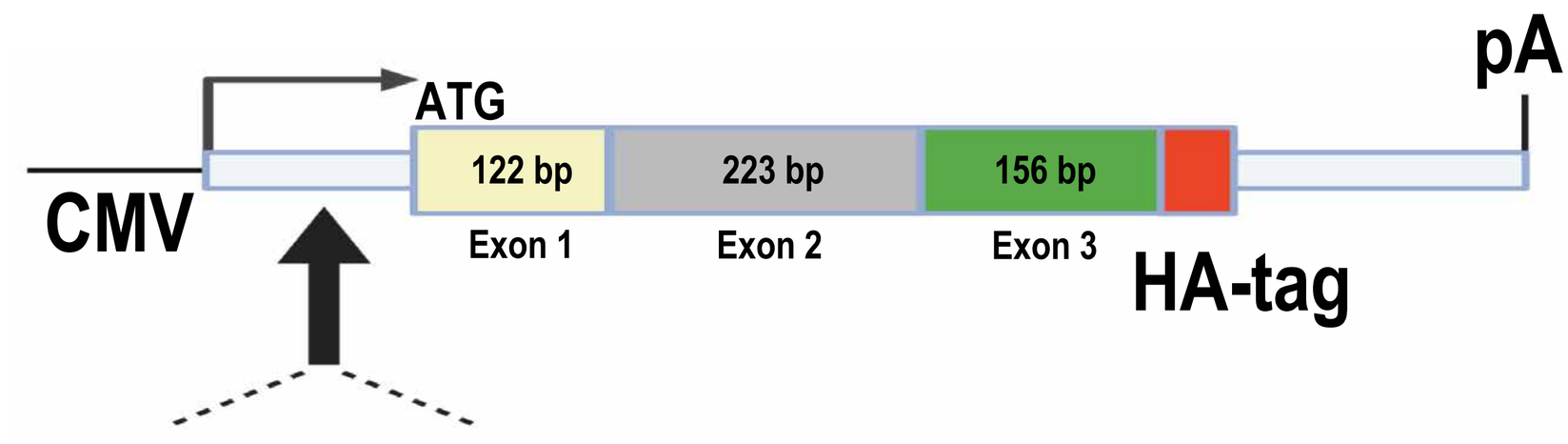

CAR-E (CCAGTTCCTG) x16

CAR-E mut (ggAGTTCCTG) x16

B

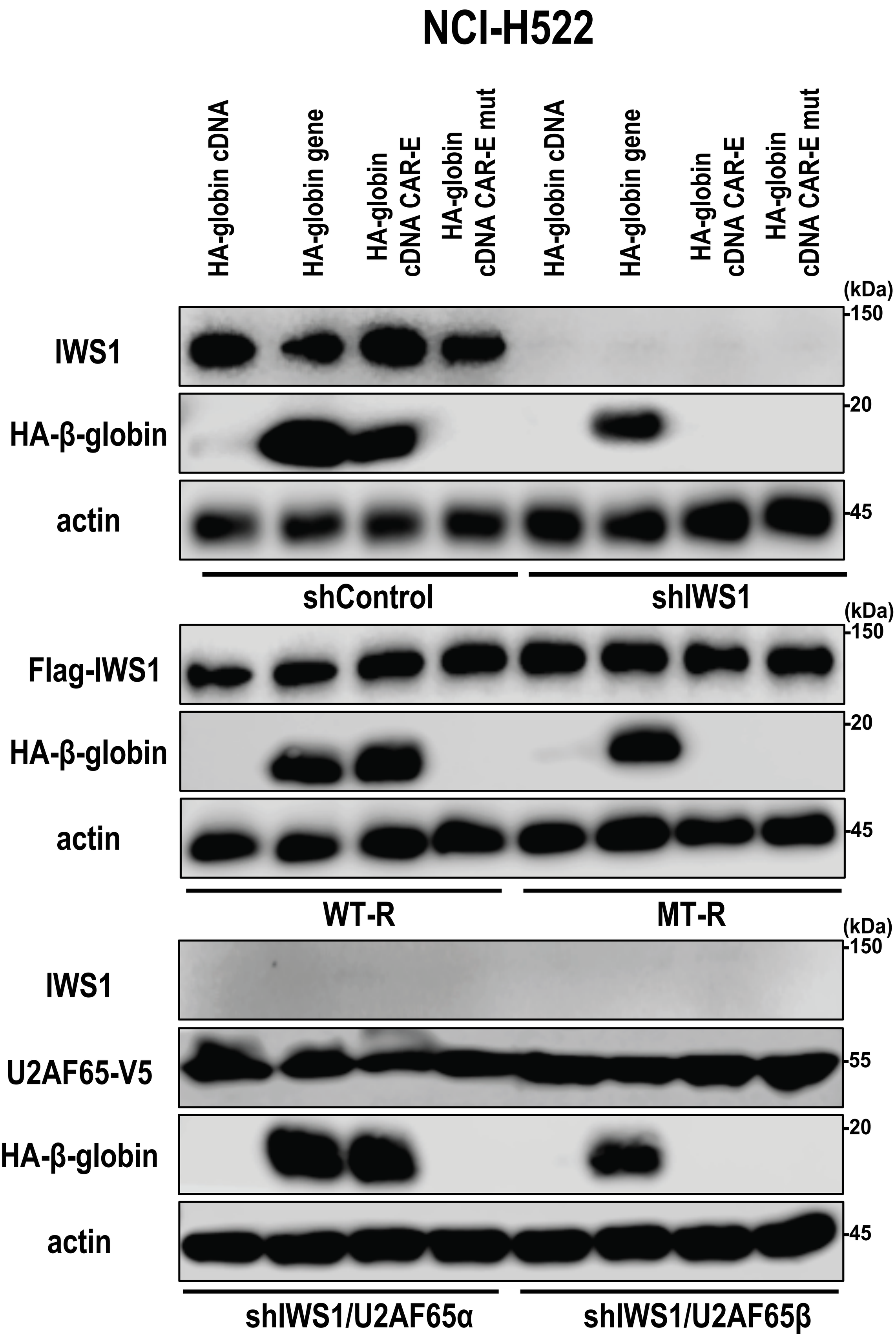

Figure 3. IWS1 phosphorylation is required for the proper function of the CAR-E elements.

A. Schematic representation of pCMV human β-globin cDNA construct indicating the position where the CAR-E and CAR-E_{mut} were inserted, as described before (Lei et al., 2013[13]). The start codon (ATG), HA tag and BGH polyA signal (pA) are indicated. The exon sizes (in bp) are shown.

B. *IWS1 phosphorylation is required for CAR-E function.* NCI-H522 cells transduced with the indicated constructs, were transfected transiently with pCMV HA-β-globin cDNA, HA-β-globin wt, HA-β-globin CAR-E and HA-β-globin CAR-E_{mut}. After 48h were harvested, and their lysates were probed with the indicated antibodies.

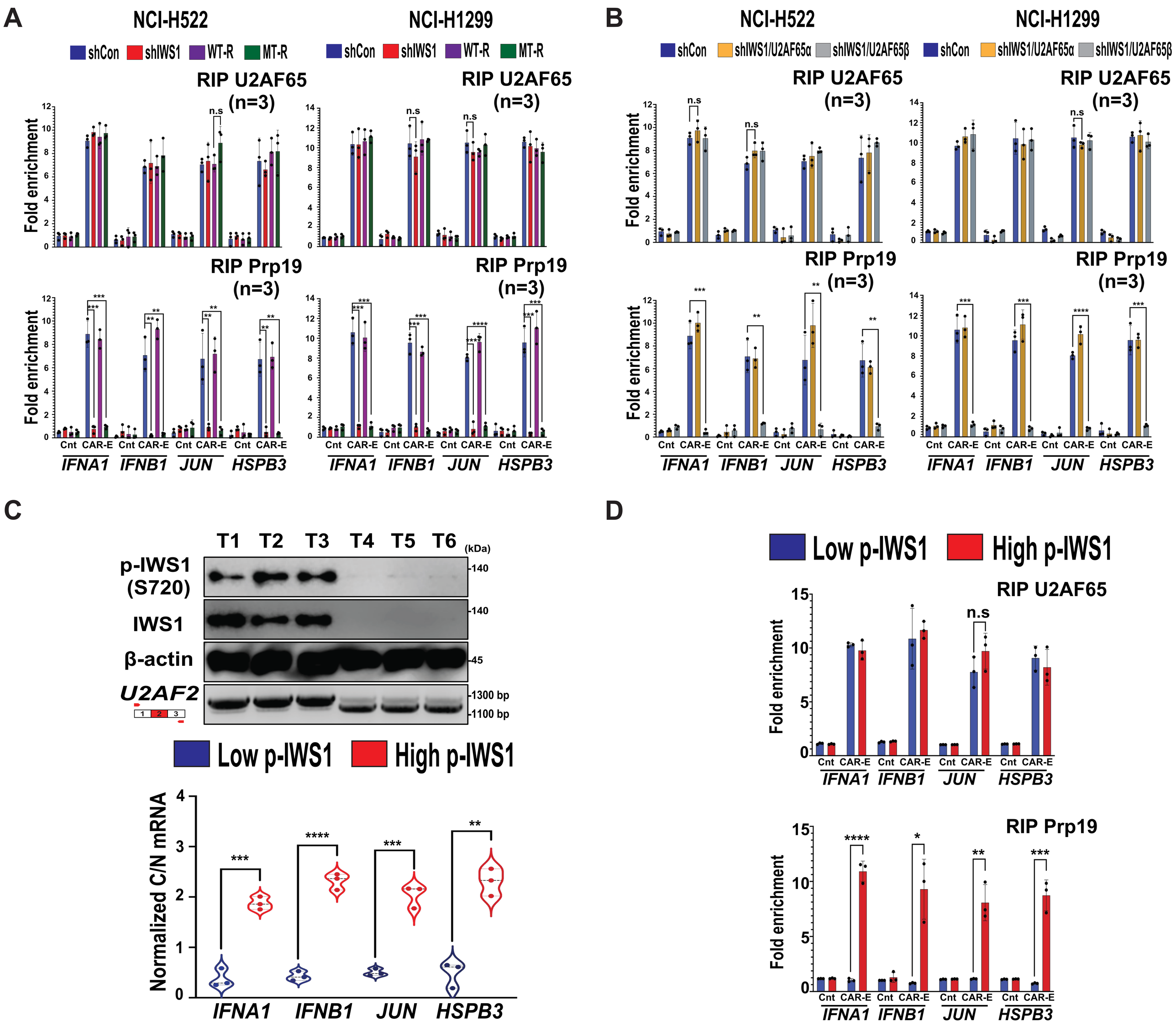
A
NCI-H522
NCI-H1299
shCon
shIWS1
WT-R
MT-R
RIP U2AF65 (n=3)
RIP Prp19 (n=3)
Fold enrichment
n.s
Cnt
CAR-E
IFNA1
IFNB1
JUN
HSPB3
B
shIWS1/U2AF65α
shIWS1/U2AF65β
C
T1
T2
T3
T4
T5
T6
(kDa)
p-IWS1 (S720)
IWS1
β-actin
U2AF2
140
45
1300 bp
1100 bp
Low p-IWS1
High p-IWS1
Normalized C/N mRNA
D

Figure 4. The splicing of the *U2AF2* mRNA downstream of IWS1 phosphorylation, regulates the Prp19 recruitment on the CAR-E elements.

A. and B. *IWS1 phosphorylation controls Prp19 recruitment on CAR-E elements.* RIP assays in NCI-H522 and NCI-H1299 cells transduced with the indicated constructs, show that whereas the binding of Prp19 to the CAR-E elements depends on the phosphorylation of IWS1, the binding of U2AF65 does not. The bars show the mean fold enrichment in U2AF65 (upper) and Prp19 (lower panel) binding in the indicated regions (anti-U2AF65 or anti-Prp19 IP, vs IgG control IP) ± SD. Data were normalized relative to the input (2%). The primer location within the intronless genes is described in Figure S4A.

C. *IWS1 phosphorylation regulates the nucleocytoplasmic export of intronless mRNAs in patients with Lung Adenocarcinoma. (*Upper panel) Western blots of lysates of 6 human LUAD samples with high and low IWS1 expression, as previously identified (Laliotis et al., 2020[15]), were probed with anti-IWS1, anti-p-IWS1 and anti-β-actin (control) antibodies. (first three lanes). RT-PCR of *U2AF2*, using oligonucleotide primers that map in exons 1 and 3 (forth lane). (Lower Panel) LUAD tumor samples were fractionated into cytoplasmic and nuclear fractions. *IFNA1, IFNB1, JUN, HSPB3* and *GAPDH* mRNA levels in each fraction were determined using qRT–PCR. For each transcript, values are represented as cytoplasmic to nuclear ratios and were normalized to 18S rRNA. The accuracy of the fractionation was validated with the experiment in Figure S4B. Bars show the mean normalized Cytosolic/Nuclear ratio ±SD

D. *IWS1 phosphorylation controls Prp19 recruitment on CAR-E in patients with Lung Adenocarcinoma.* RIP assays in the same high and low-IWS1 group, show that whereas the binding of Prp19 to the CAR-E elements depends on the phosphorylation of IWS1, the binding of U2AF65 does not. The bars show the mean fold enrichment in U2AF65 (upper) and Prp19 (lower panel) binding in the indicated regions (anti-U2AF65 or anti-Prp19 IP, vs IgG control IP) ± SD. Data were normalized relative to the input (2%).

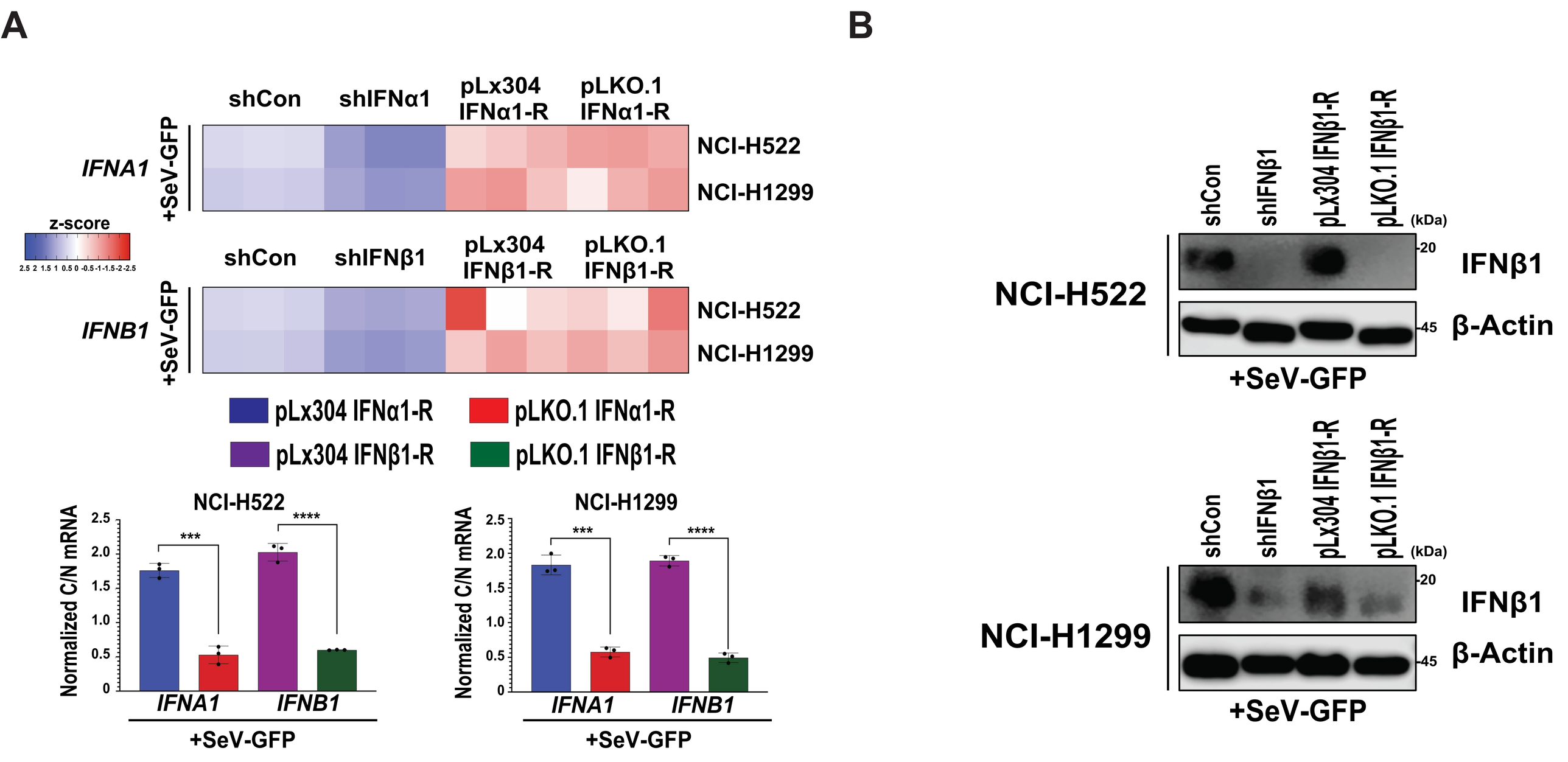
A
shCon
shIFNα1
pLx304 IFNα1-R
pLKO.1 IFNα1-R
IFNA1
+SeV-GFP
NCI-H522
NCI-H1299
z-score
2.5 2 1.5 1 0.5 0 -0.5 -1 -1.5 -2 -2.5
shCon
shIFNβ1
pLx304 IFNβ1-R
pLKO.1 IFNβ1-R
IFNB1
+SeV-GFP
NCI-H522
NCI-H1299
pLx304 IFNα1-R
pLKO.1 IFNα1-R
pLx304 IFNβ1-R
pLKO.1 IFNβ1-R
NCI-H522
Normalized C/N mRNA
2.5
2.0
1.5
1.0
0.5
0
***
****
IFNA1
IFNB1
+SeV-GFP
NCI-H1299
Normalized C/N mRNA
2.5
2.0
1.5
1.0
0.5
0
***
****
IFNA1
IFNB1
+SeV-GFP
B
shCon
shIFNβ1
pLx304 IFNβ1-R
pLKO.1 IFNβ1-R
(kDa)
NCI-H522
20
IFNβ1
45
β-Actin
+SeV-GFP
shCon
shIFNβ1
pLx304 IFNβ1-R
pLKO.1 IFNβ1-R
(kDa)
NCI-H1299
20
IFNβ1
45
β-Actin
+SeV-GFP

Figure 5. RNA-Pol II affects the splicing-independent nuclear export of intronless genes.

A. *RNA Pol II contributes to the nucleocytoplasmic export of intronless genes* (Upper panel) Total RNA was harvested from NCI-H522 and NCI-H1299 cells, transduced with the indicated constructs. The construct maps for the pLx304 (RNA Pol II-driven) or pLKO.1 (RNA Pol III-driven) can be found in Fig. S5A. The expression of *IFNA1 and IFNB1,* mRNAs was determined by qRT-PCR and normalized to 18S rRNA levels. The results are represented as heatmap using z-scores from three individual biological experiments. For type I IFN induction SeV infection was performed. (Lower panel) The same cells were fractionated into cytoplasmic and nuclear fractions, *IFNA1, IFNB1* and *GAPDH* mRNA levels in each fraction were determined using qRT–PCR. For each transcript, values are represented as cytoplasmic to nuclear ratios and were normalized to 18S rRNA. For type I IFN induction SeV-GFP infection was performed. The accuracy of the fractionation was validated with the experiment in Figure S5B. Bars show the mean normalized Cytosolic/Nuclear ratio ±SD

B. Western blots of lysates of NCI-H522 and NCI-H1299 cells, transduced with the indicated constructs, were probed with anti-IFNβ1 and anti-β-actin (control) antibodies. For type I IFN induction SeV-GFP infection was performed. In this figure, NCI-H522 and NCI-H1299 cells were infected with MOI of 0.5 for 16h and MOI of 0.25 for 24h of SeV-GFP virus, respectively. All assays in this figure were done in triplicate, on three biological replicates. n.s : non-significant *$p<0.05$, **$p<0.01$, ***$p<0.001$, ****$p<0.0001$. (one-side unpaired t-test).

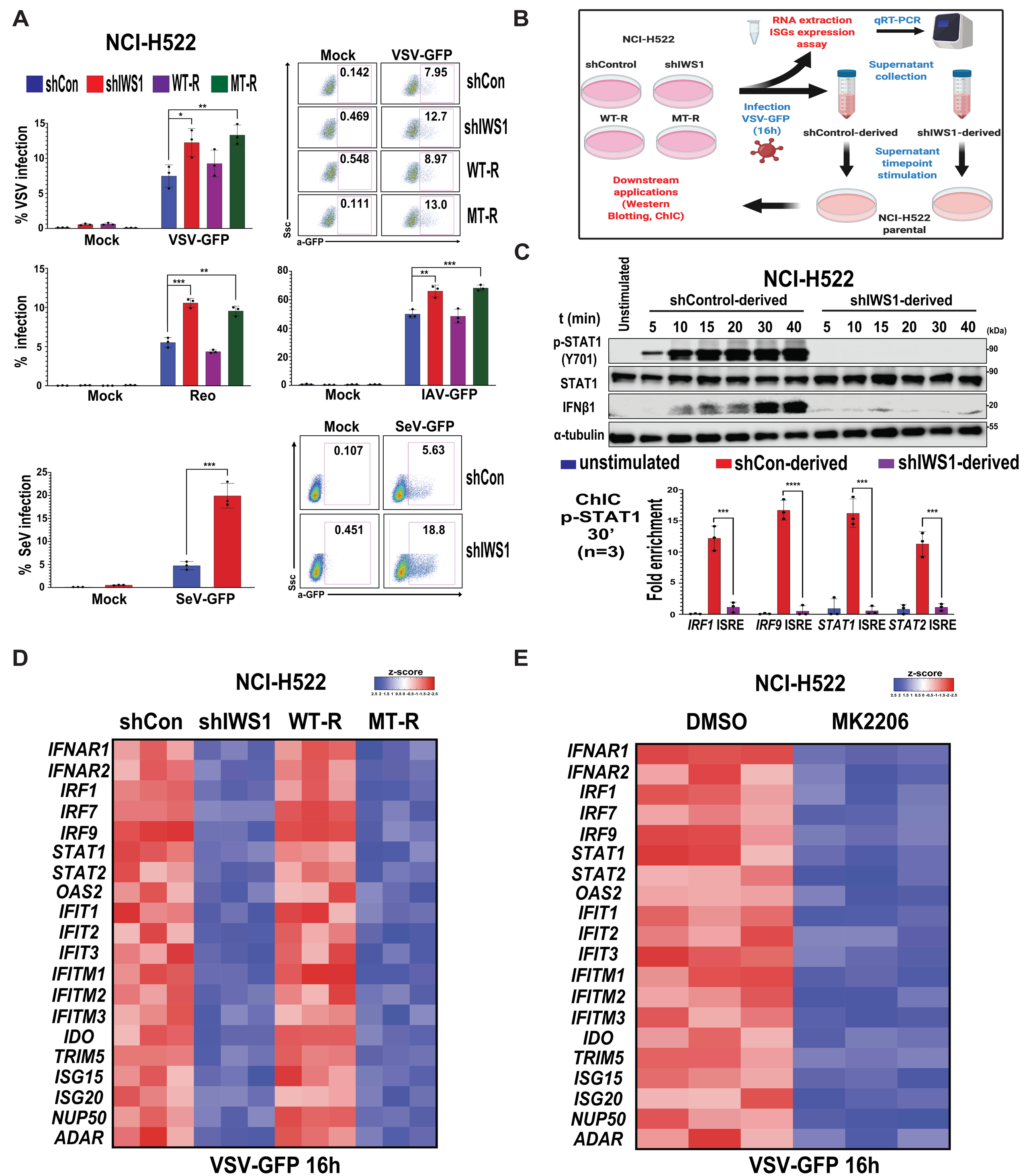
A
NCI-H522
shCon
shIWS1
WT-R
MT-R
% VSV infection
Mock
VSV-GFP
Mock
VSV-GFP
0.142
7.95
0.469
12.7
0.548
8.97
0.111
13.0
Ssc
a-GFP
% infection
Mock
Reo
Mock
IAV-GFP
% SeV infection
Mock
SeV-GFP
Mock
SeV-GFP
0.107
5.63
0.451
18.8
B
NCI-H522
shControl
shIWS1
WT-R
MT-R
RNA extraction
ISGs expression
assay
qRT-PCR
Supernatant
collection
Infection
VSV-GFP
(16h)
shControl-derived
shIWS1-derived
Supernatant
timepoint
stimulation
Downstream
applications
(Western
Blotting, ChIC)
NCI-H522
parental
C
NCI-H522
Unstimulated
shControl-derived
shIWS1-derived
t (min)
5 10 15 20 30 40
5 10 15 20 30 40
(kDa)
p-STAT1
(Y701)
STAT1
IFNβ1
α-tubulin
unstimulated
shCon-derived
shIWS1-derived
ChIC
p-STAT1
30'
(n=3)
Fold enrichment
IRF1 ISRE
IRF9 ISRE
STAT1 ISRE
STAT2 ISRE
D
NCI-H522
z-score
shCon
shIWS1
WT-R
MT-R
IFNAR1
IFNAR2
IRF1
IRF7
IRF9
STAT1
STAT2
OAS2
IFIT1
IFIT2
IFIT3
IFITM1
IFITM2
IFITM3
IDO
TRIM5
ISG15
ISG20
NUP50
ADAR
VSV-GFP 16h
E
NCI-H522
z-score
DMSO
MK2206
IFNAR1
IFNAR2
IRF1
IRF7
IRF9
STAT1
STAT2
OAS2
IFIT1
IFIT2
IFIT3
IFITM1
IFITM2
IFITM3
IDO
TRIM5
ISG15
ISG20
NUP50
ADAR
VSV-GFP 16h

Figure 6. The loss of IWS1 phosphorylation enhances viral infection, through the aberrant p-STAT1 signaling and transcription of ISGs.

A. *The loss of IWS1 phosphorylation enhances viral replication.* The indicated NCI-H522 cells were infected with VSV-GFP, SeV-GFP, Reovirus or Influenza A-GFP at an MOI of 0.5 for 16 hours (VSV-GFP and IAV-GFP), MOI of 1 for 24h hours (SeV-GFP and Reovirus), respectively. Cells were then fixed and were examined for GFP positivity (for VSV, SeV and Flu) to measure the percentage of cells infected using flow cytometry. For Reovirus, the fixed-infected cells were stained with anti-reovirus antibody, followed by anti-mouse Alexa488-conjugated secondary antibody, and analyzed as well with Flow cytometry. Results shown are representative of at least three independent experiments, each performed with triplicate samples. Bars show the % infection of each viral strain ±SD.

B. *Summary of the experimental design.* NCI-H522 shControl, shIWS1, shIWS1/WT-R and shIWS1/MT-R cells were infected with VSV-GFP at an MOI of 0.5 for 16h. Then the cells were harvested for RNA and their supernatant was collected. The RNA was used for downstream qRT-PCR applications. The supernatant derived from shControl and shIWS1 was used to stimulate NCI-H522 parental cells in time point intervals. These cells were used for Chromatin Immuno Cleavage (ChIC) or were harvested for protein.

C. *Loss of IWS1 phosphorylation impairs p-STAT1 activation following viral infection.* (Upper panel) NCI-H522 parental cells were stimulated for the indicated time point intervals with shControl and shIWS1-derived supernatant and were harvested for protein. In parallel experiments, NCI-H522 unstimulated parental cells were harvested as control. The protein lysates were probed with the indicated antibodies. (Lower panel) ChIC assays showing the binding of p-STAT1 in the *ISRE of IRF1, IRF9, STAT1 and STAT2* genes, in NCI-H522 cells following stimulation for 30' with shControl and shIWS1-derived supernatant. In parallel experiments, NCI-

H522 unstimulated parental cells were proceeded as control. The bars show the mean fold enrichment in p-STAT1 binding in the indicated regions ±SD, relative to IgG IP.

D. *Loss of AKT/p-IWS1 axis impairs the ISG transcription following viral infection.* Total RNA was harvested from NCI-H522 cells, transduced with the indicated constructs following VSV-GFP infection at MOI 0.5 for 16h. The expression of 20 ISGs mRNAs was determined by qRT-PCR and normalized to 18S rRNA. The results are represented as heatmap using z-scores from three individual biological experiments.

E. Total RNA was harvested from NCI-H522 cells, treated with DMSO or 5μM of the pan-AKT inhibitor MK2206, following VSV-GFP infection at MOI x for 16h. The expression of 20 ISGs mRNAs was determined by qRT-PCR and normalized to 18S rRNA. The results are represented as heatmap using z-scores from three individual biological experiments. All assays in this figure were done in triplicate, on three biological replicates. n.s : non-significant *$p<0.05$, **$p<0.01$, ***$p<0.001$, ****$p<0.0001$. (one-side unpaired t-test).

A

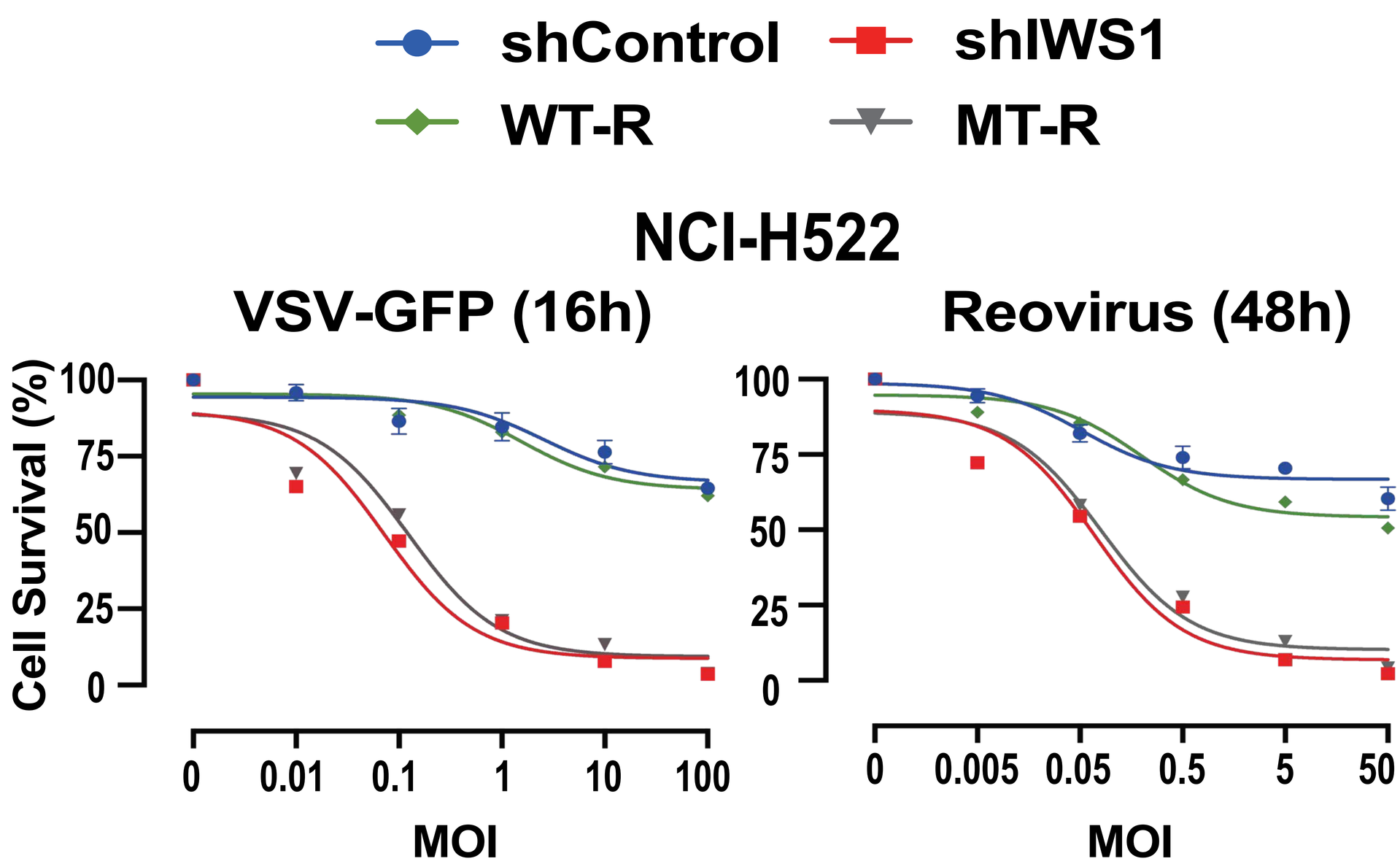
shControl
shIWS1
WT-R
MT-R
NCI-H522
VSV-GFP (16h)
Reovirus (48h)
Cell Survival (%)
100
75
50
25
0
0
0.01
0.1
1
10
100
MOI
0
0.005
0.05
0.5
5
50
MOI

B

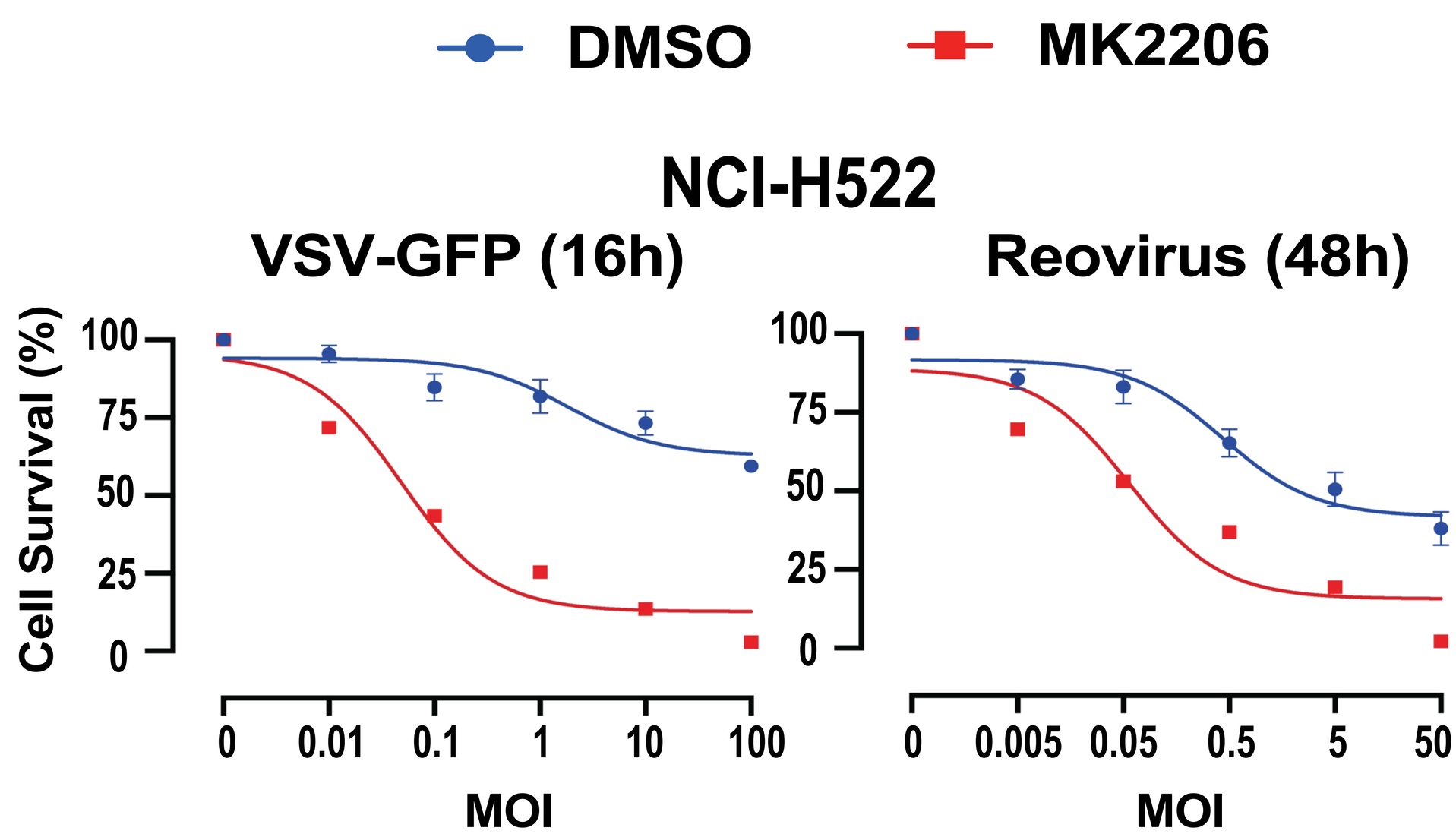
DMSO
MK2206
NCI-H522
VSV-GFP (16h)
Reovirus (48h)
Cell Survival (%)
100
75
50
25
0
0
0.01
0.1
1
10
100
MOI
0
0.005
0.05
0.5
5
50
MOI

C

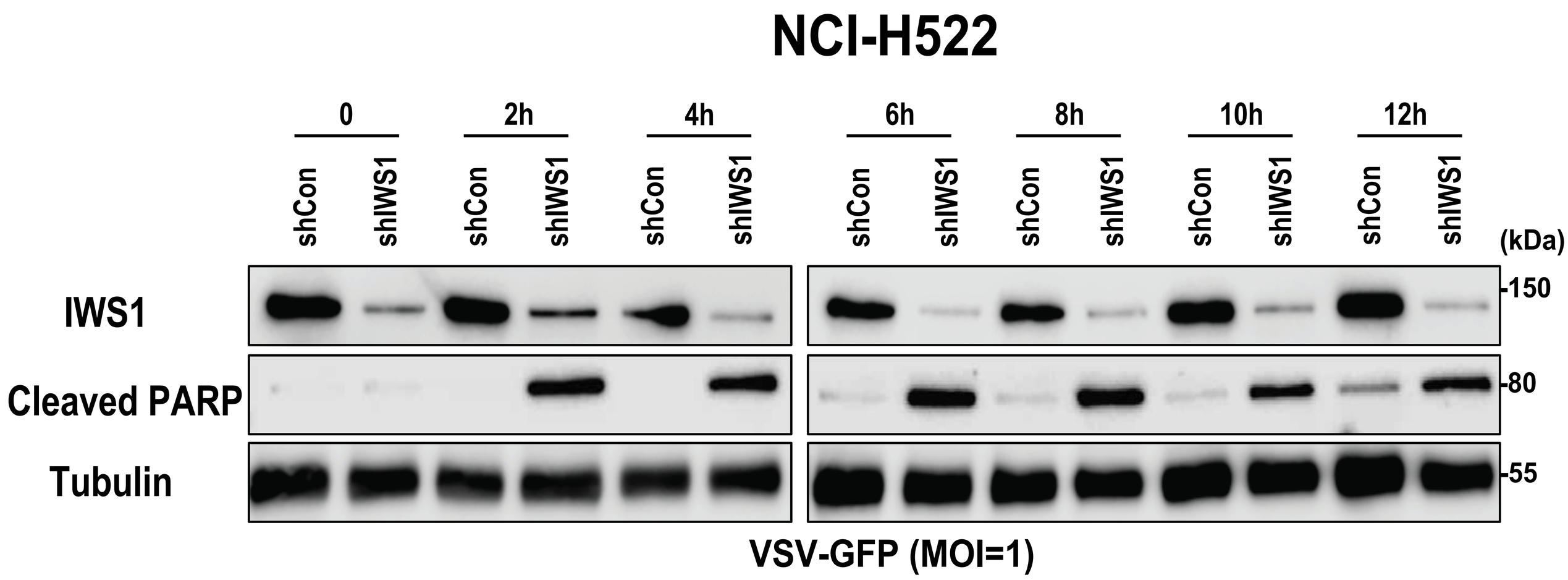
NCI-H522
0
2h
4h
6h
8h
10h
12h
shCon
shIWS1
(kDa)
IWS1
Cleaved PARP
Tubulin
150
80
55
VSV-GFP (MOI=1)

Figure 7. Inhibition of the AKT/p-IWS1 axis sensitizes lung adenocarcinoma cells to oncolytic viral killing.

A. *The loss of IWS1 phosphorylation sensitizes lung adenocarcinoma cells to oncolytic viral killing.* NCI-H522 cells transduced with the indicated constructs were exposed to increasing MOI of VSV-GFP or Reovirus for 16h and 48h, respectively. Cell proliferation was assessed by fluorescent detection of the reduction of resazurin to resorufin by viable cells and expressed as a percentage of uninfected cells. Mean values are shown ±SD (n=3) and data are representative of two independent experiments.

B. *The loss of AKT/p-IWS1 axis sensitizes lung adenocarcinoma cells to oncolytic viral killing.* NCI-H522 cells treated with DMSO or 5μM of the pan-AKT inhibitor MK2206, were exposed to increasing MOI of VSV-GFP or Reovirus for 16h and 48h, respectively. Cell proliferation was assessed by fluorescent detection of the reduction of resazurin to resorufin by viable cells and expressed as a percentage of uninfected cells. Mean values are shown ±SD (n=3) and data are representative of two independent experiments.

C. *The loss of IWS1 phosphorylation sensitizes lung adenocarcinoma cells to oncolytic viral killing via Caspase-mediated death.* NCI-H522 shControl and shIWS1 cells were infected for the indicated time point intervals with VSV-GFP at a MOI=1. Western blot lysates from these time points were probed with the indicated antibodies, showing a robust cleavage of PARP, a sensitive marker of Caspase mediated apoptosis, in shIWS1 cells even in early time points of infections.

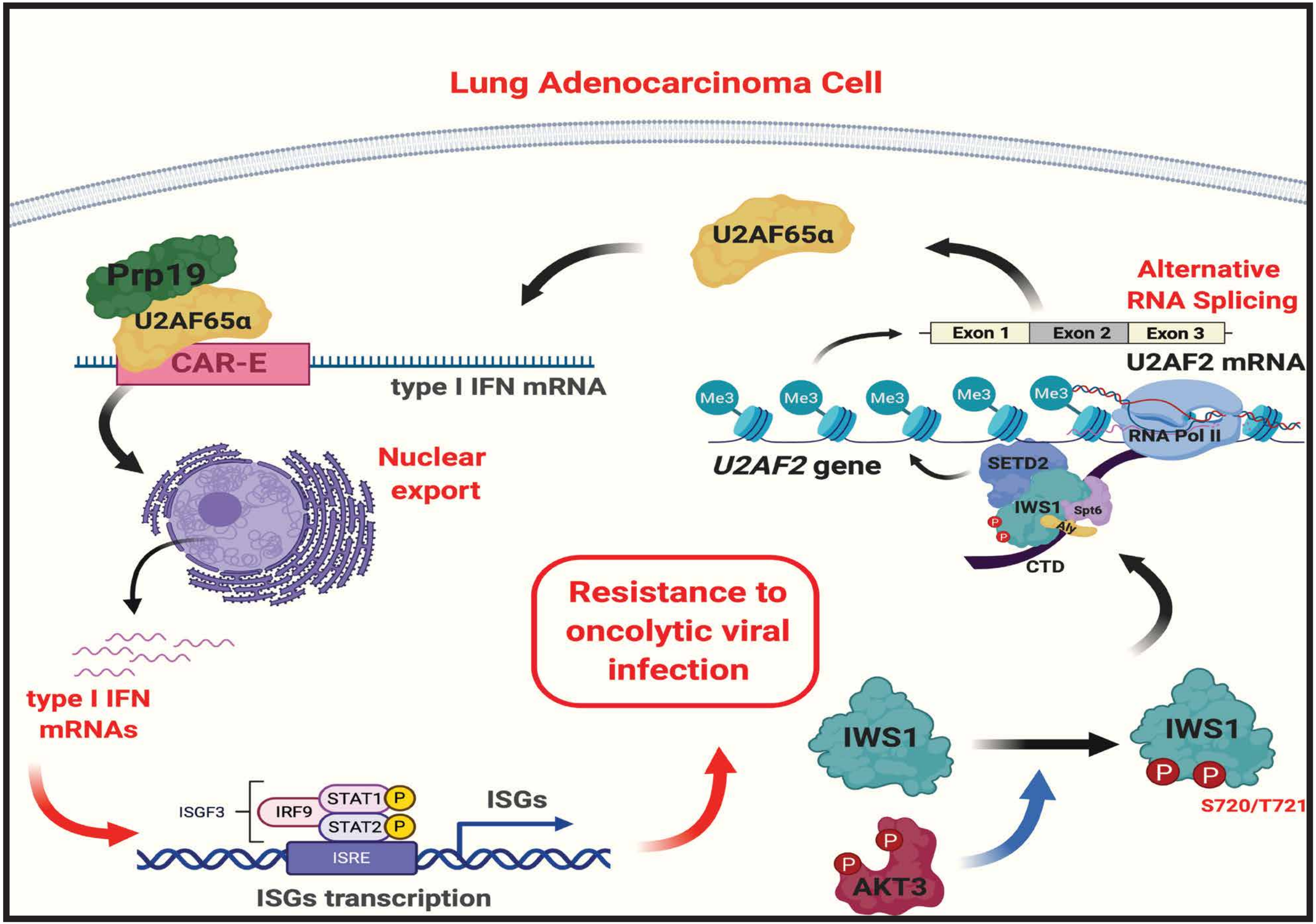
Lung Adenocarcinoma Cell
U2AF65α
Prp19
U2AF65α
CAR-E
type I IFN mRNA
Nuclear export
type I IFN mRNAs
ISGF3
IRF9
STAT1
P
STAT2
P
ISRE
ISGs
ISGs transcription
Resistance to oncolytic viral infection
Alternative RNA Splicing
Exon 1
Exon 2
Exon 3
U2AF2 mRNA
Me3
Me3
Me3
Me3
Me3
RNA Pol II
U2AF2 gene
SETD2
IWS1
Spt6
Aly
P
P
CTD
IWS1
P
AKT3
IWS1
P
P
S720/T721

Figure 8. Model of the effect of IWS1 phosphorylation at S720/721, on type I IFN expression and response to oncolytic viral infection.

A. *Model of the effect of IWS1 phosphorylation at S720/721, on type I IFN expression and response to oncolytic viral infection.* The phosphorylation of IWS1 at S720/T721 by AKT kinase controls the epigenetic regulation of *U2AF2* alternative RNA splicing, leading to inclusion of exon 2 in the mature *U2AF2* mRNA. Subsequently, the U2AF65α isoform binds CAR-E of type I IFNs and recruits Prp19, promoting their nucleocytoplasmic export and expression. During oncolytic viral infection, type I IFNs are properly exported and expressed, leading to p-STAT1 activation and assembly of the ISGF3 on ISGs promoters. This confers resistance of lung adenocarcinoma cells to oncolytic viral infection.

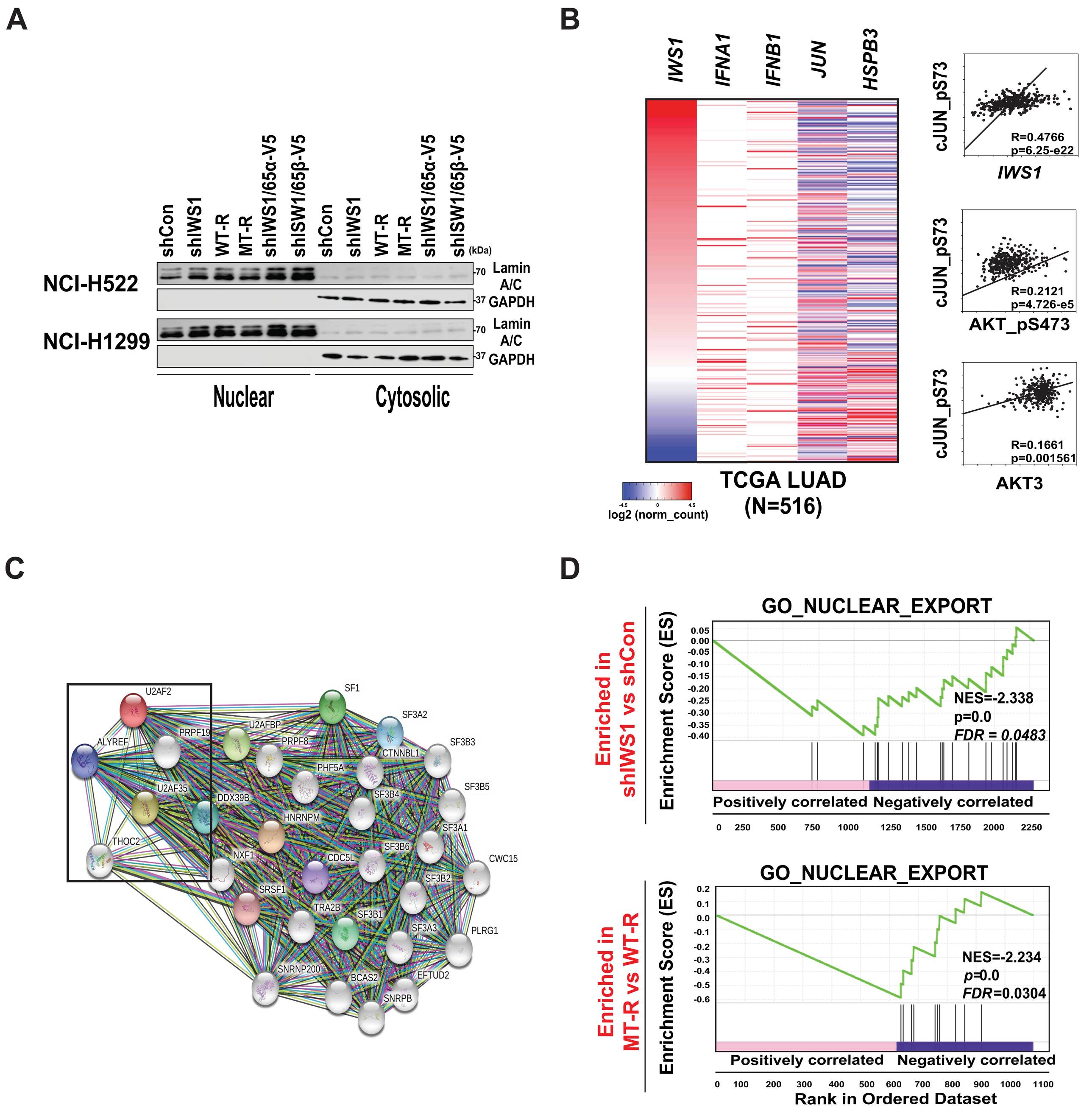
A
shCon
shIWS1
WT-R
MT-R
shIWS1/65α-V5
shISW1/65β-V5
(kDa)
NCI-H522
NCI-H1299
70
37
Lamin A/C
GAPDH
Nuclear
Cytosolic
B
IWS1
IFNA1
IFNB1
JUN
HSPB3
TCGA LUAD
(N=516)
log2 (norm_count)
-4.5
0
4.5
cJUN_pS73
IWS1
R=0.4766
p=6.25-e22
AKT_pS473
R=0.2121
p=4.726-e5
AKT3
R=0.1661
p=0.001561
C
U2AF2
SF1
SF3A2
U2AFBP
PRPF19
ALYREF
PRPF8
SF3B3
CTNNBL1
PHF5A
U2AF35
SF3B5
DDX39B
SF3B4
HNRNPM
SF3A1
THOC2
SF3B6
NXF1
CDC5L
CWC15
SF3B2
SRSF1
TRA2B
SF3B1
SF3A3
PLRG1
SNRNP200
BCAS2
EFTUD2
SNRPB
D
GO_NUCLEAR_EXPORT
Enriched in shIWS1 vs shCon
Enrichment Score (ES)
NES=-2.338
p=0.0
FDR = 0.0483
Positively correlated
Negatively correlated
GO_NUCLEAR_EXPORT
Enriched in MT-R vs WT-R
Enrichment Score (ES)
NES=-2.234
p=0.0
FDR=0.0304
Positively correlated
Negatively correlated
Rank in Ordered Dataset

Figure S1 (relative to Figure 1). IWS1 phosphorylation regulates the nucleocytoplasmic transport of mRNAs transcribed from a set of intronless genes, via *U2AF2* alternative RNA splicing.

A. The cytosolic and nuclear compartment of the indicated NCI-H522 (upper two lines) and NCI-H1299 cells (lower two lines) were probed with the indicated antibodies, to validate the fractionation.

B. (Left panel) Heat Maps showing the correlation of IWS1 RNA levels with intronless genes in the TCGA LUAD database. The RNA-seq expression values from each individual patient were expressed as $\log_2$ normalized counts and they were used to calculate the correlation coefficients. (Right panel) Correlation coefficient graphs of Reverse Phase Protein Assay (RPPA) levels of p-c-Jun (S73) in TCGA LUAD with the RNA levels of IWS1 (top), RRPA levels p-AKT (S473) (middle) and RNA levels of AKT3 (lower).

C. The Protein-Protein Interaction (PPI) network analysis of U2AF65-Prp19 using the STRING database. U2AF65 and Prp19 interact with components of TREX complex and Ref/Aly controlling the export of naturally intronless genes (red box)

D. Gene Set Enrichment Analysis (GSEA) of genes differentially expressed in shIWS1 versus shControl (left panels) and in shIWS1/MT-R versus shIWS1/WT-R (right panels) NCI-H522 cells demonstrates significant enrichment in genes involved in Nuclear Export. (NES–normalized enrichment score, FDR–false discovery ratio)

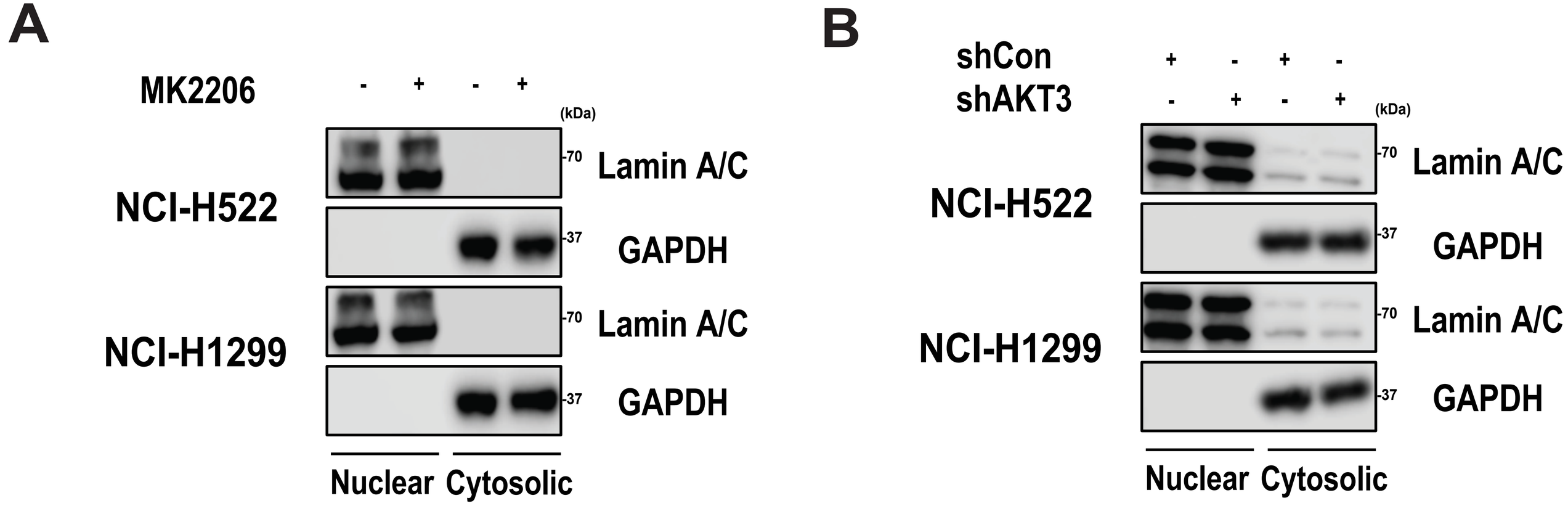
A
MK2206
- + - +
(kDa)
NCI-H522
-70
Lamin A/C
-37
GAPDH
NCI-H1299
-70
Lamin A/C
-37
GAPDH
Nuclear Cytosolic
B
shCon
shAKT3
+ - + -
- + - +
(kDa)
NCI-H522
-70
Lamin A/C
-37
GAPDH
NCI-H1299
-70
Lamin A/C
-37
GAPDH
Nuclear Cytosolic

Figure S2 (relative to Figure 2). AKT3 kinase affects the nucleocytoplasmic export of RNAs transcribed from intronless genes, thought IWS1 phosphorylation.

A and B. The cytosolic and nuclear compartment of the indicated NCI-H522 (upper two lines) and NCI-H1299 cells (lower two lines) were probed with the indicated antibodies, to validate the fractionation.

A

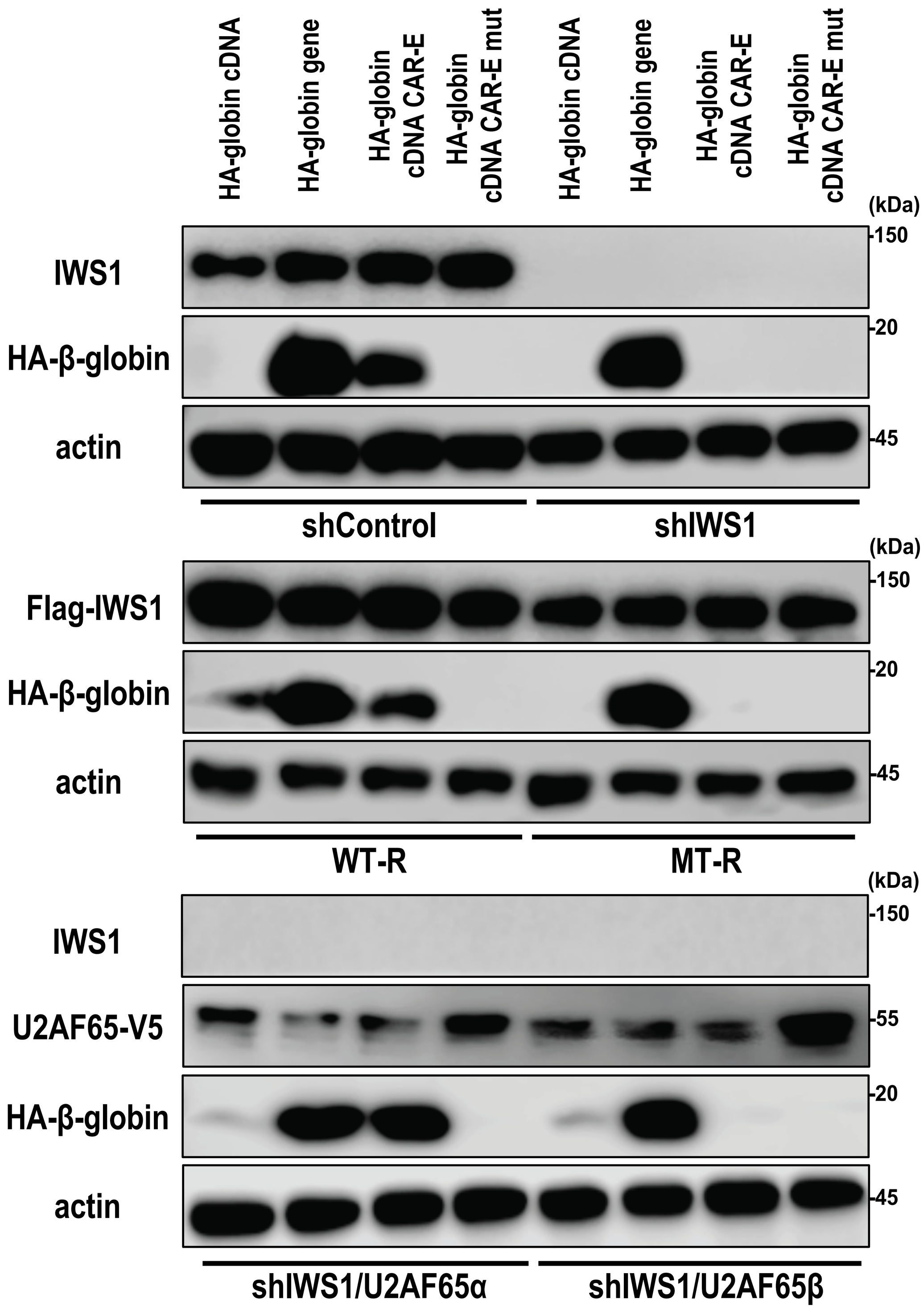
NCI-H1299
HA-globin cDNA
HA-globin gene
HA-globin cDNA CAR-E
HA-globin cDNA CAR-E mut
HA-globin cDNA
HA-globin gene
HA-globin cDNA CAR-E
HA-globin cDNA CAR-E mut
(kDa)
IWS1
150
HA-β-globin
20
actin
45
shControl
shIWS1
(kDa)
Flag-IWS1
150
HA-β-globin
20
actin
45
WT-R
MT-R
(kDa)
IWS1
150
U2AF65-V5
55
HA-β-globin
20
actin
45
shIWS1/U2AF65α
shIWS1/U2AF65β

Figure S3 (relative to Figure 3). IWS1 phosphorylation is required for the proper function of the CAR-E elements.

A. *IWS1 phosphorylation is required for CAR-E function.* NCI-H1299 cells transduced with the indicated constructs, were transfected transiently with pCMV HA-β-globin cDNA, HA-β-globin wt, HA-β-globin CAR-E and HA-β-globin CAR-E_{mut}. After 48h were harvested, and their lysates were probed with the indicated antibodies.

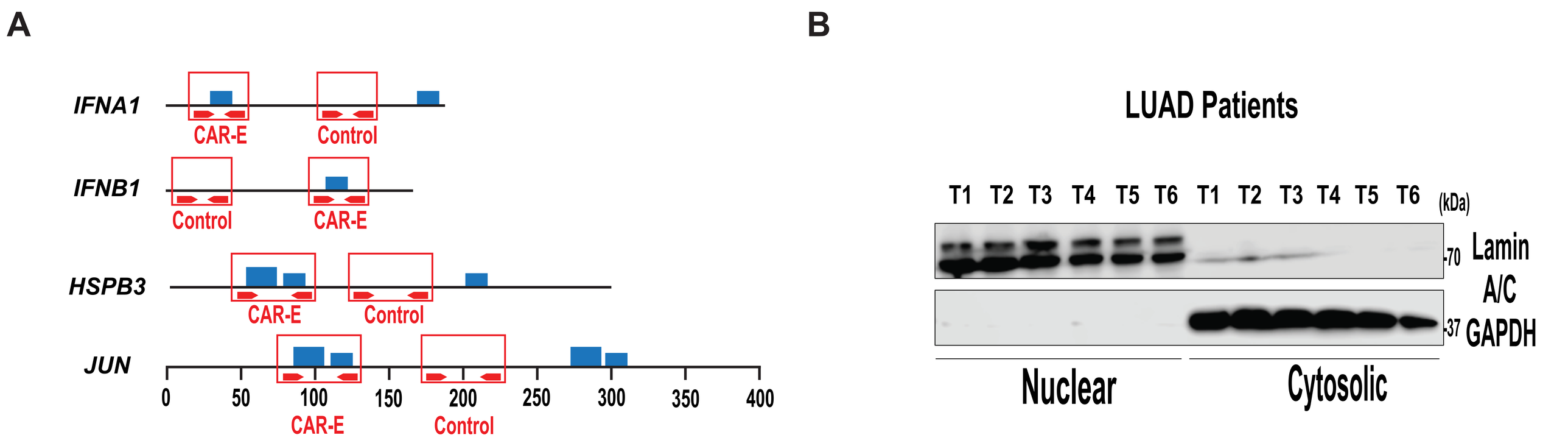
A
IFNA1
CAR-E
Control
IFNB1
Control
CAR-E
HSPB3
CAR-E
Control
JUN
0
50
100
150
200
250
300
350
400
CAR-E
Control
B
LUAD Patients
T1 T2 T3 T4 T5 T6 T1 T2 T3 T4 T5 T6
(kDa)
70
Lamin A/C
37
GAPDH
Nuclear
Cytosolic

Figure S4 (relative to Figure 4). The splicing of the *U2AF2* mRNA downstream of IWS1 phosphorylation, regulates the Prp19 recruitment on the CAR-E elements.

A. The 10-nt consensus element (CAR-E) identified in the CARs from *IFNα1, IFNβ1, c-Jun or HSPB3* is shown, as described previously (Lei et al., 2013[13]). The locations of the CAR-Es in each CAR are indicated by the boxes. The numbering is relative to the first nucleotide of each CAR sequence. In red boxes with the red arrows shows the primers used to amplify the CAR-E elements (CAR-E) or the control binding regions (Control) in the indicated genes.

B. The cytosolic and nuclear compartment of the indicated low and high-IWS1 LUAD group were probed with the indicated antibodies, to validate the fractionation.

A

CMV_promoter (RNA Pol II_driven)

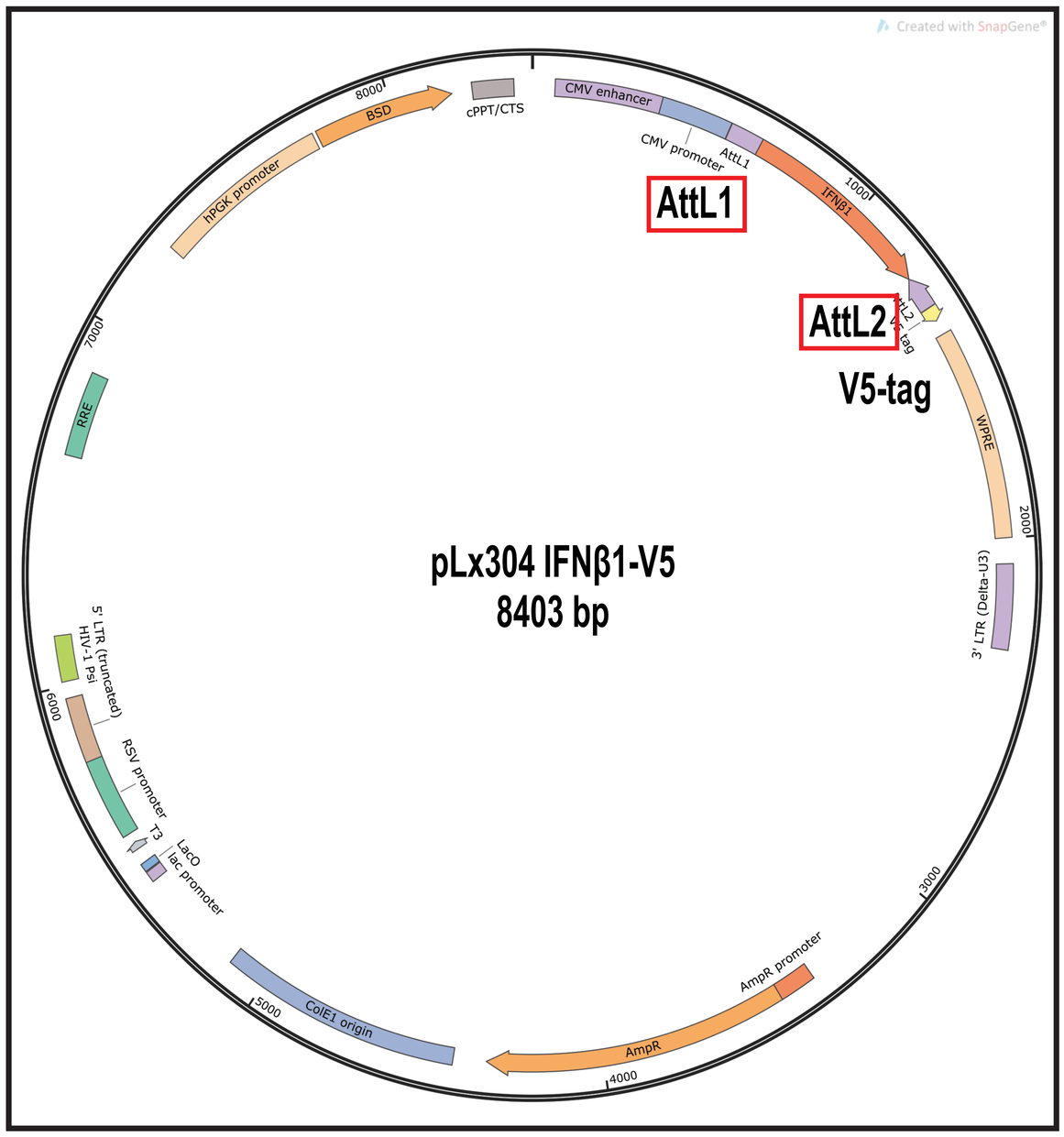

U6_promoter (RNA Pol III_driven)

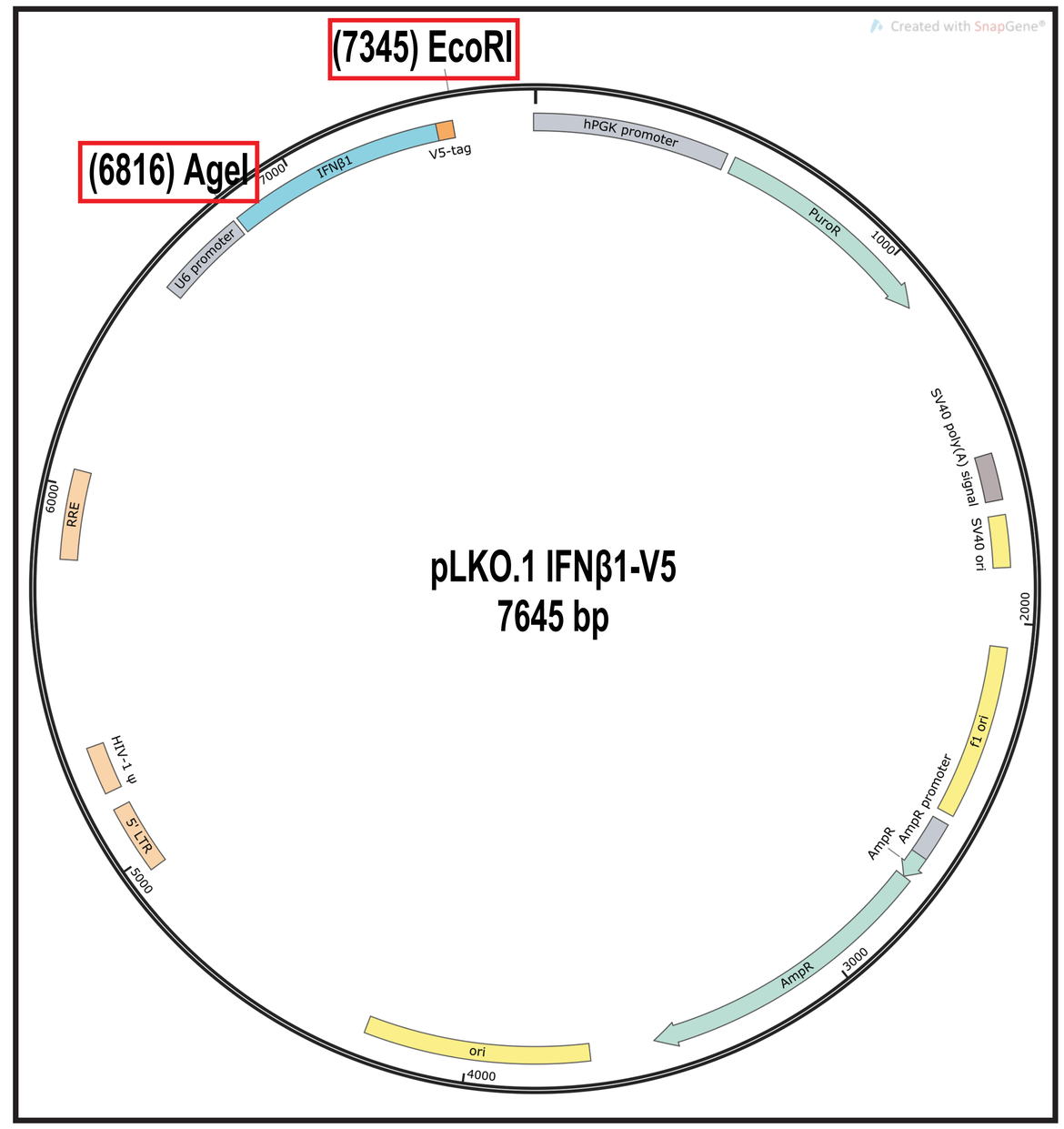

B

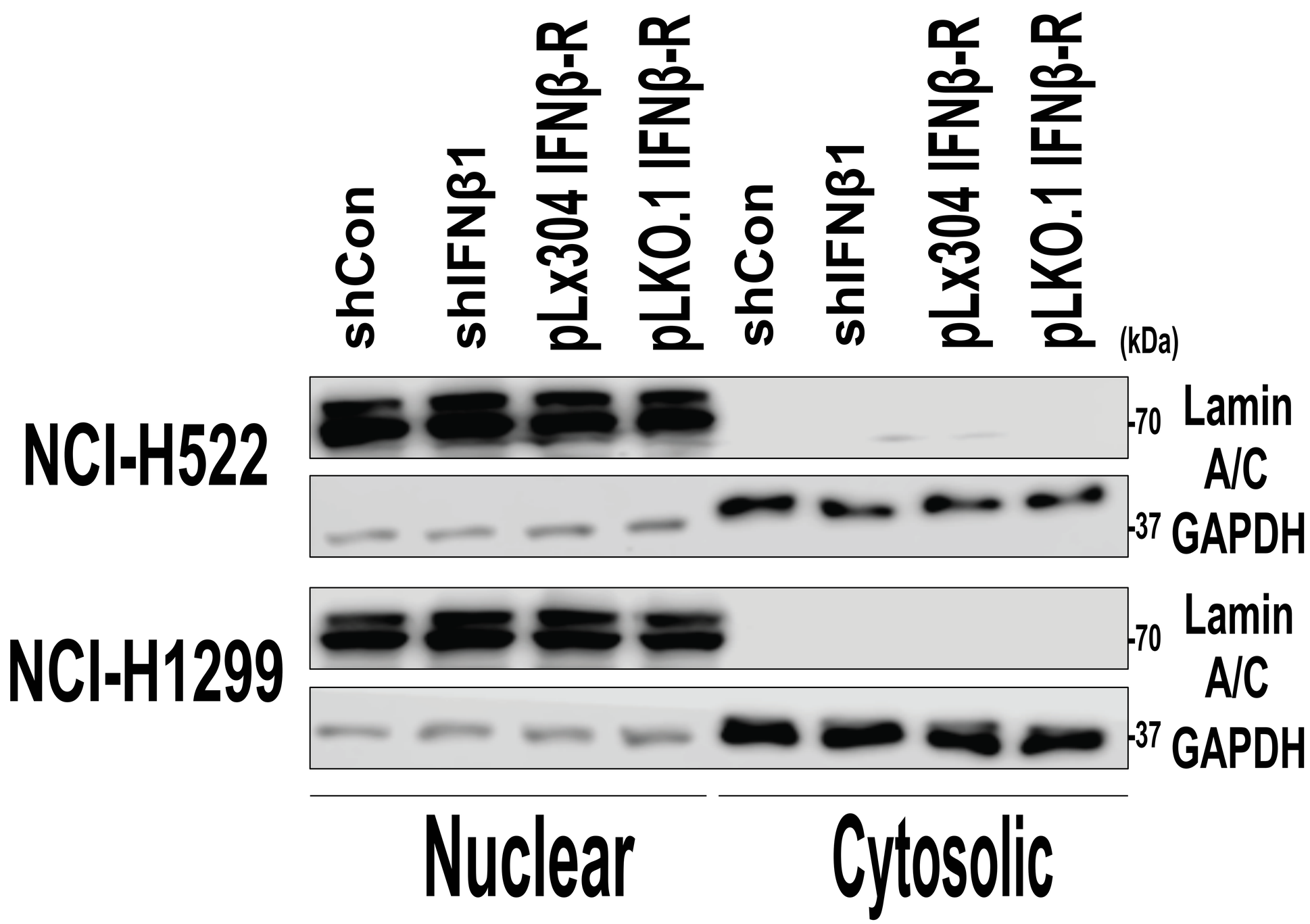

Figure S5 (relative to Figure 5). RNA-Pol II affects the splicing-independent nuclear export of intronless genes.

A. Schematic representation of CMV pLx304 IFNβ1-V5 (RNA Pol II-driven) and U6 pLKO.1 IFNβ1-V5 (RNA Pol III-driven) used in Fig. 5A and 5B is shown. The red boxes in pLx304 indicate the Gateway LR sites and in pLKO.1 map the restriction enzyme sites used for proper IFNβ1-V5 cloning into pLKO.1 (AgeI-EcoRI sites)

B. The cytosolic and nuclear compartment of the indicated NCI-H522 (upper two lines) and NCI-H1299 cells (lower two lines) were probed with the indicated antibodies, to validate the fractionation.

A

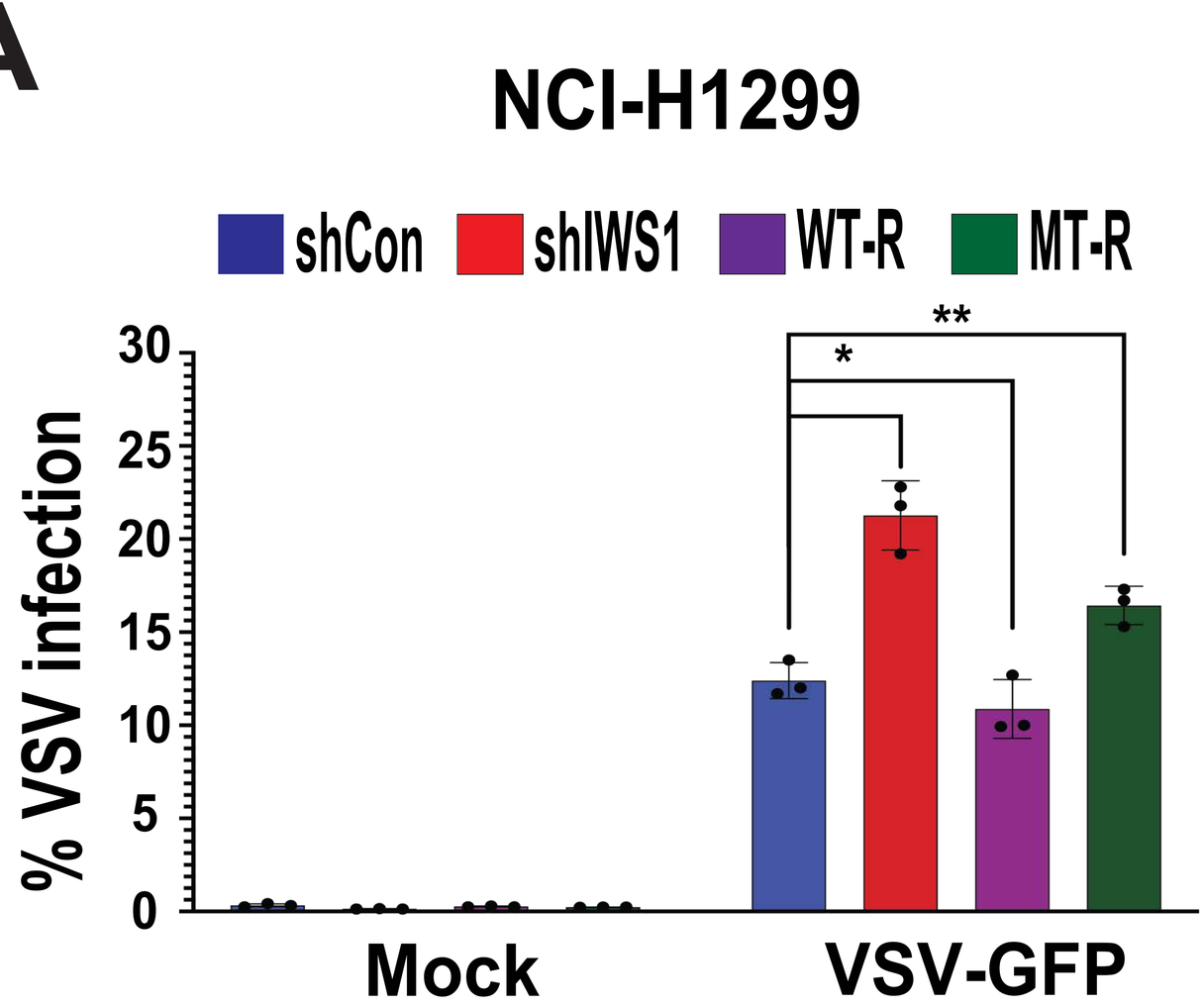
NCI-H1299
shCon
shIWS1
WT-R
MT-R
% VSV infection
30
25
20
15
10
5
0
*
**
Mock
VSV-GFP

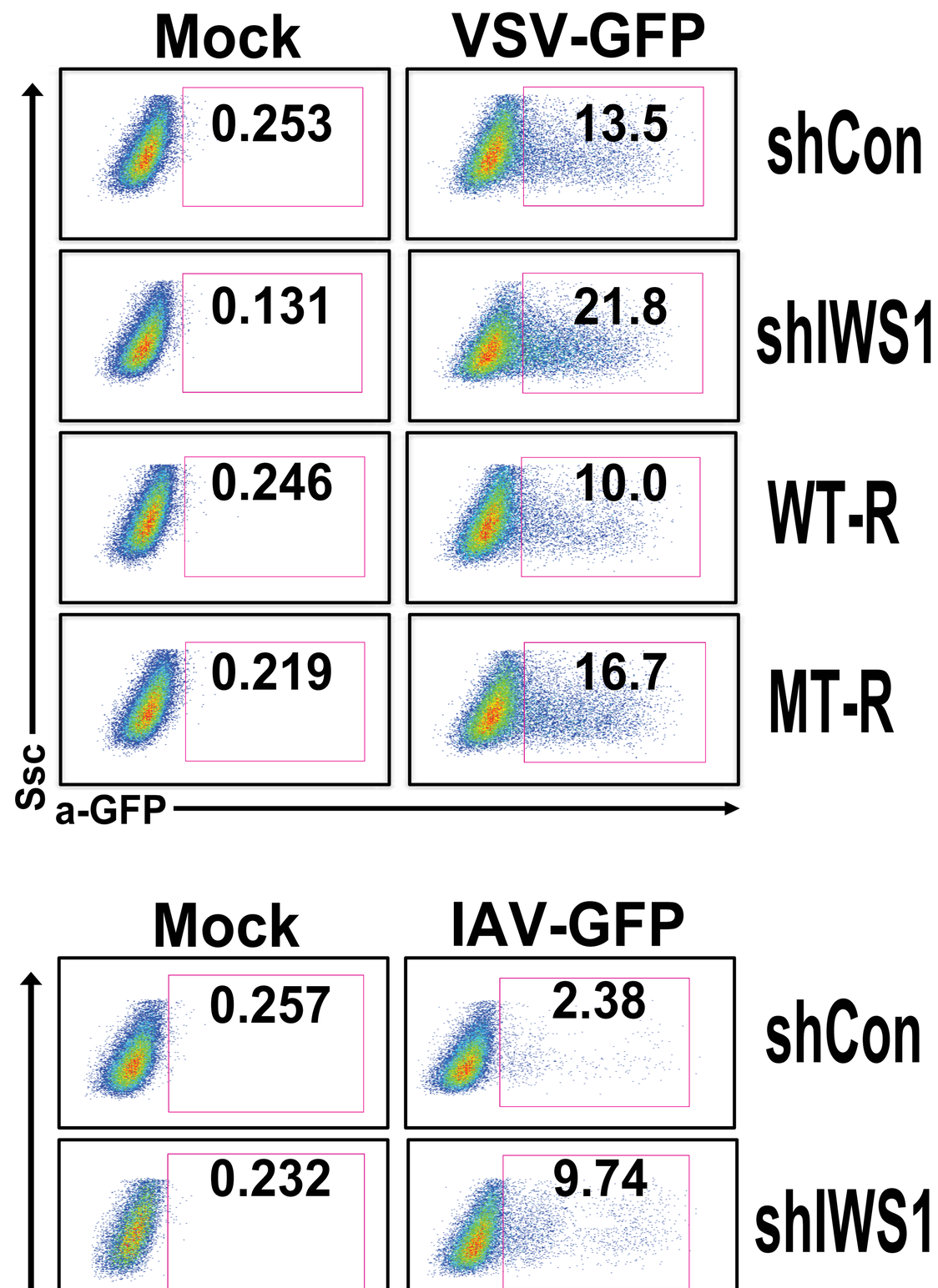
Mock
VSV-GFP
0.253
13.5
shCon
0.131
21.8
shIWS1
0.246
10.0
WT-R
0.219
16.7
MT-R
Ssc
a-GFP

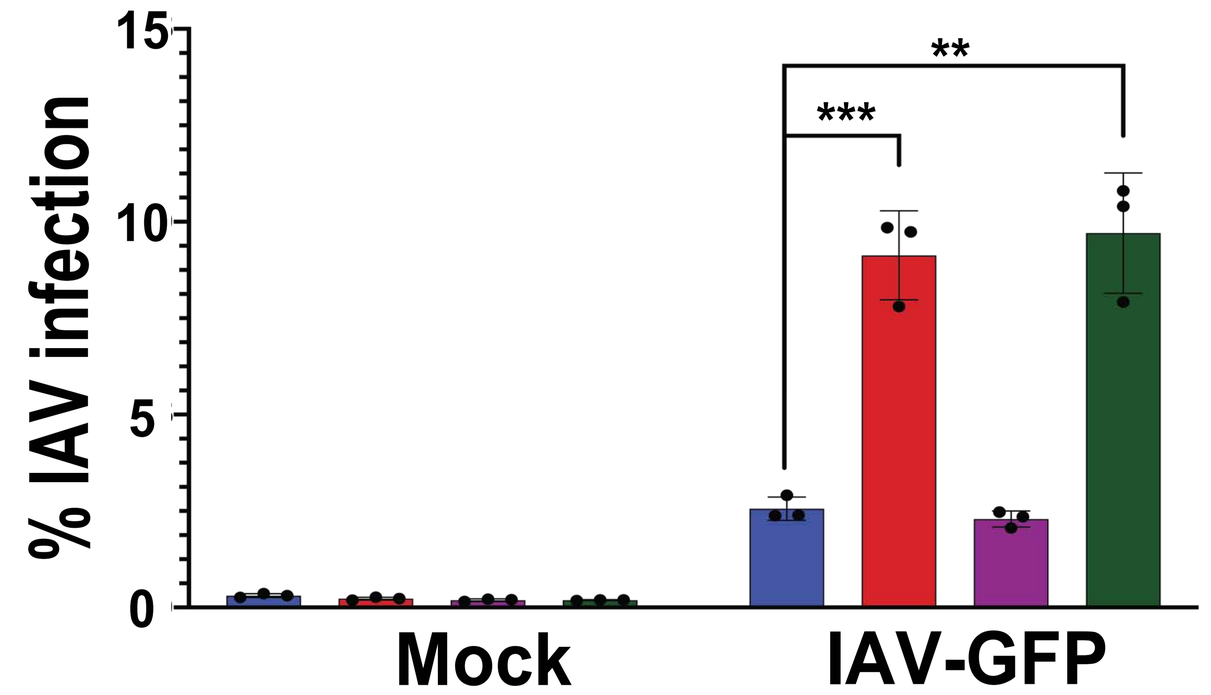
% IAV infection
15
10
5
0
***
**
Mock
IAV-GFP

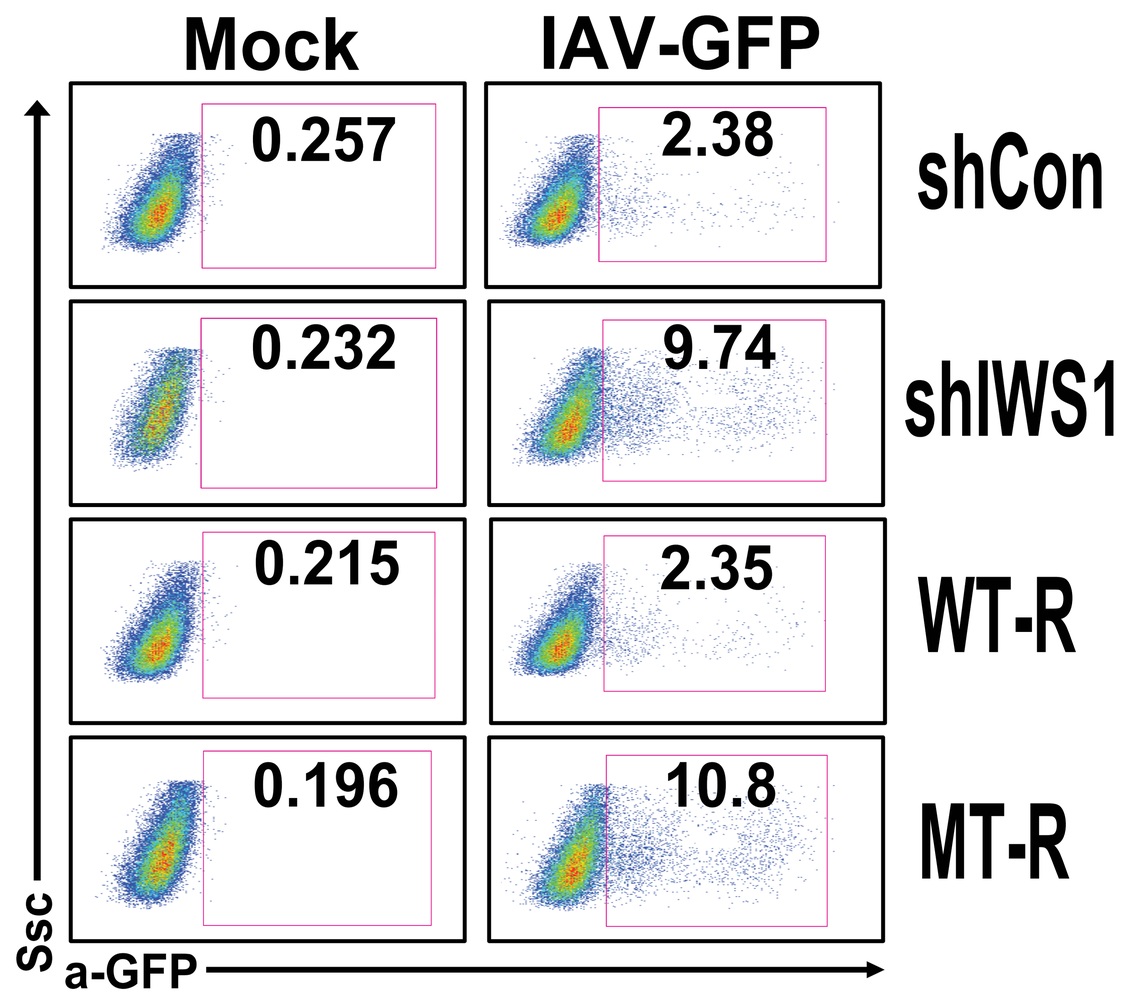
Mock
IAV-GFP
0.257
2.38
shCon
0.232
9.74
shIWS1
0.215
2.35
WT-R
0.196
10.8
MT-R
Ssc
a-GFP

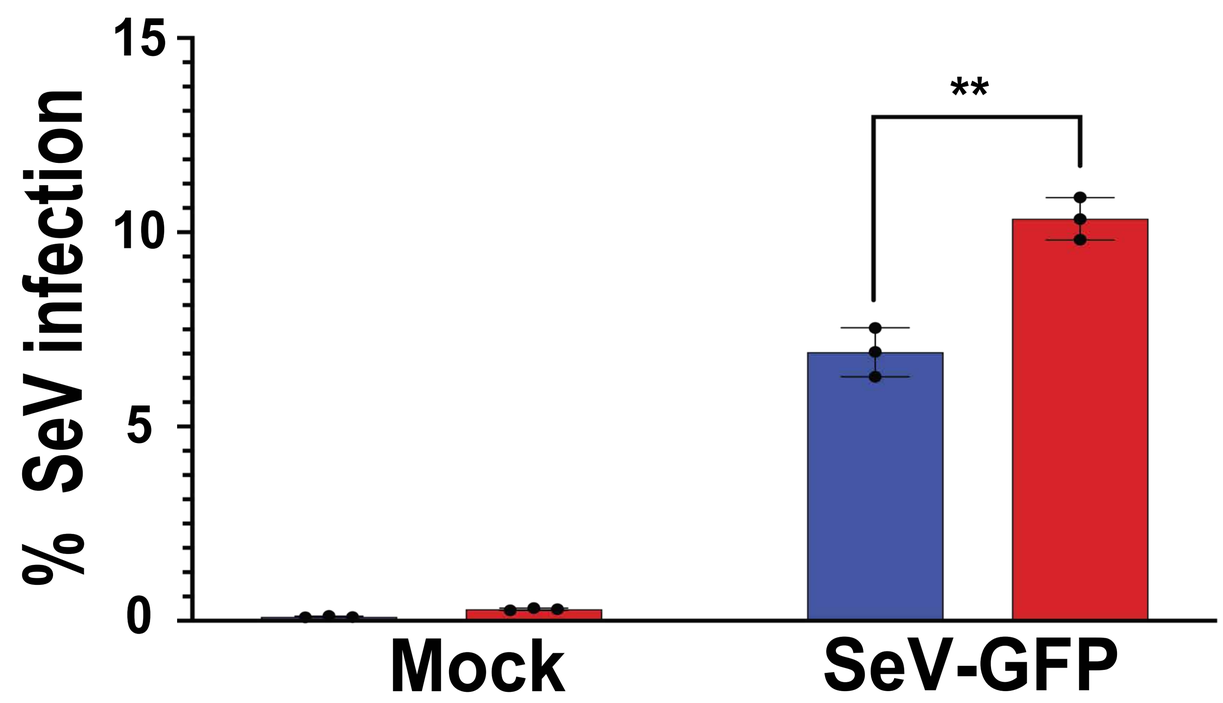
% SeV infection
15
10
5
0
**
Mock
SeV-GFP

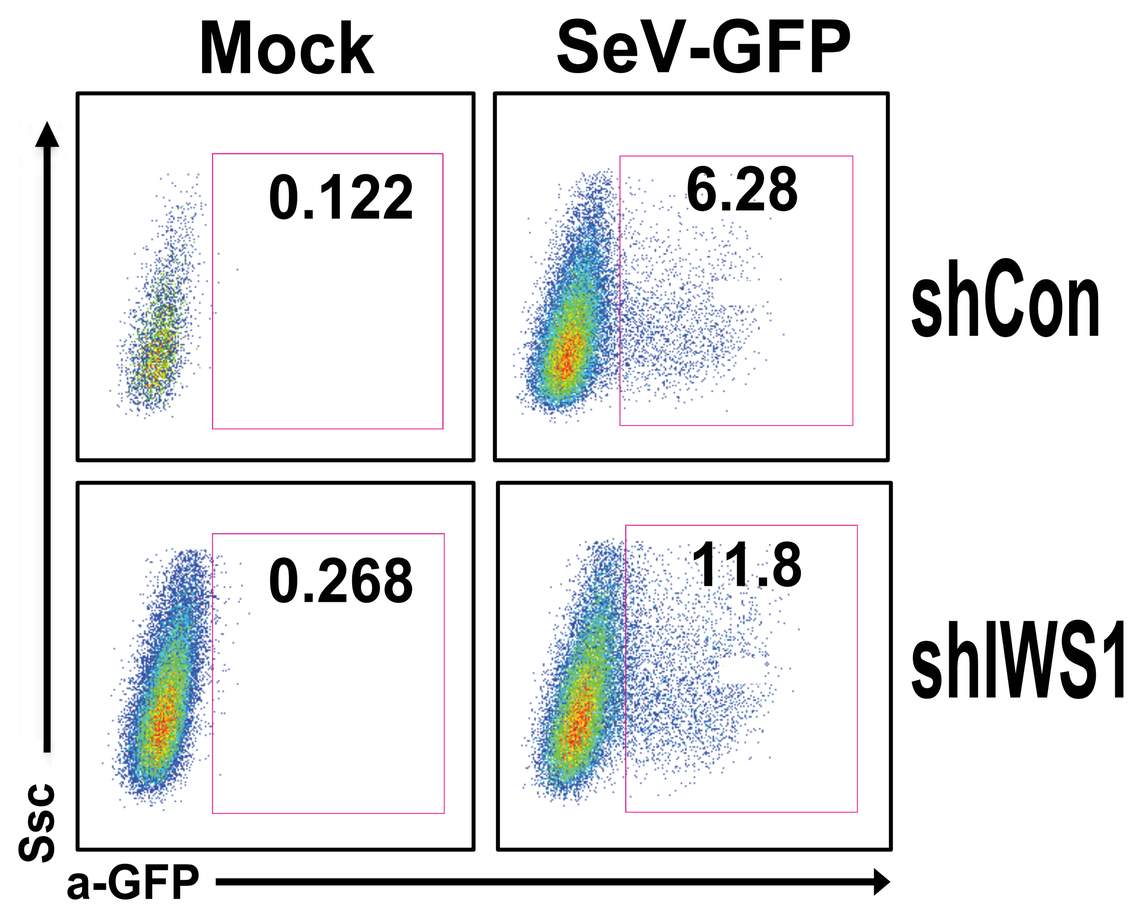
Mock
SeV-GFP
0.122
6.28
shCon
0.268
11.8
shIWS1
Ssc
a-GFP

B

IFNβ1 (1000U/mL)
Unstim.
5
10
15
20
30
40
IFNβ1
Tubulin
-20
-55
NCI-H522

Figure S6 (relative to Figure 6). The loss of IWS1 phosphorylation enhances viral replication, through the aberrant p-STAT1 signaling and transcription of ISGs.

A. *The loss of IWS1 phosphorylation enhances viral replication.* The indicated NCI-H1299 cells were infected with VSV-GFP, SeV-GFP or Influenza-GFP at an MOI of 0.25 for 24h hours (VSV-GFP and SeV-GFP) and MOI of 1 for 24 hours (IAV-GFP), respectively. Cells were then fixed and were examined for GFP positivity to measure the percentage of cells infected using flow cytometry. Results shown are representative of at least three independent experiments, each performed with triplicate samples. Bars show the % infection of each viral strain ±SD. All assays in this figure were done in triplicate, on three biological replicates. n.s : non-significant *$p<0.05$, **$p<0.01$, ***$p<0.001$, ****$p<0.0001$. (one-side unpaired t-test).

B. NCI-H522 cells were stimulated with 1000u/mL human IFNβ1 for time point intervals and their lysates were probed with the indicated antibodies. The results confirm the endocytosis of exogenous IFNβ1 in these cells.

A

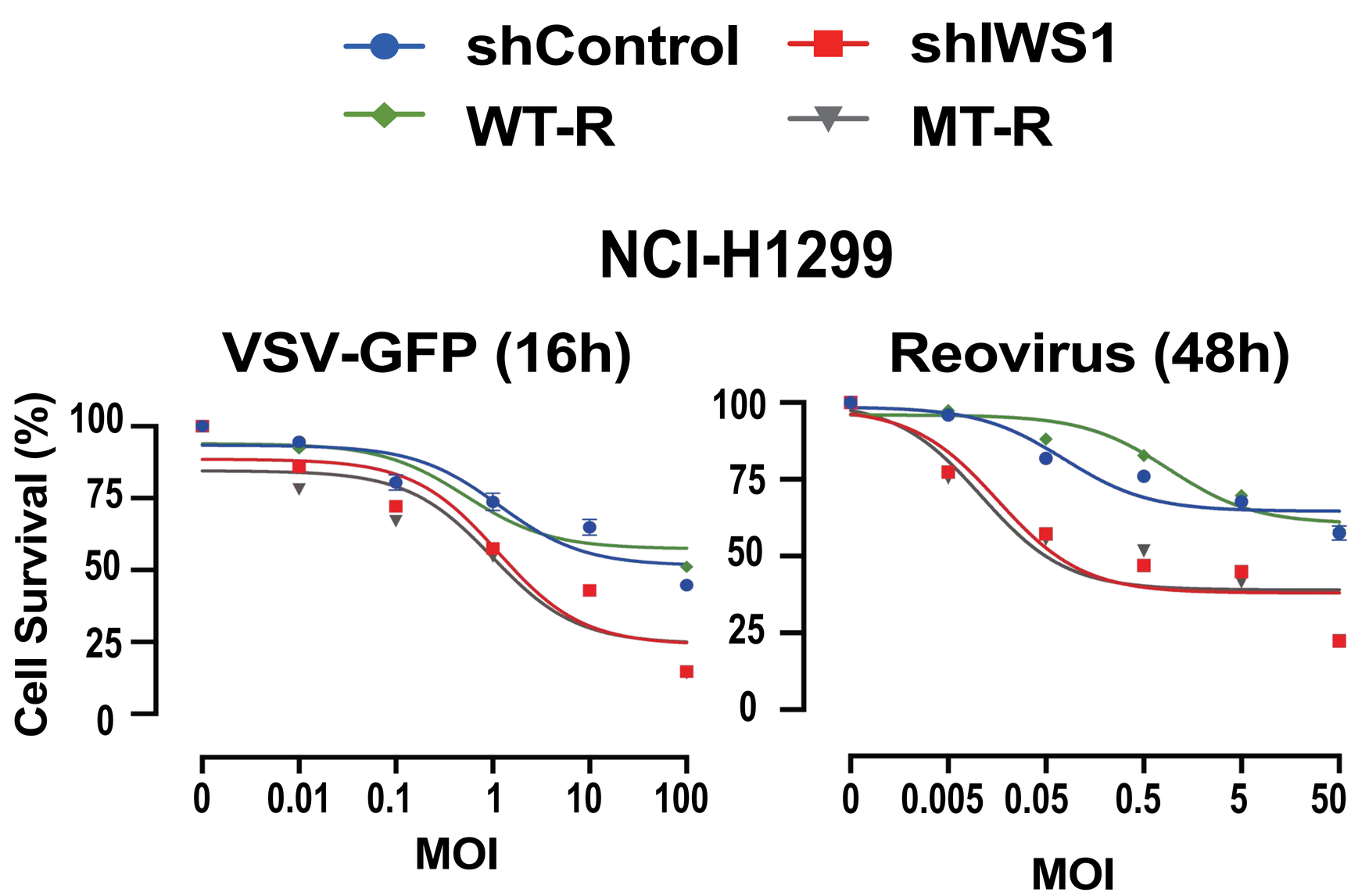
shControl
shIWS1
WT-R
MT-R
NCI-H1299
VSV-GFP (16h)
Reovirus (48h)
Cell Survival (%)
100
75
50
25
0
0
0.01
0.1
1
10
100
MOI
0
0.005
0.05
0.5
5
50
MOI

B

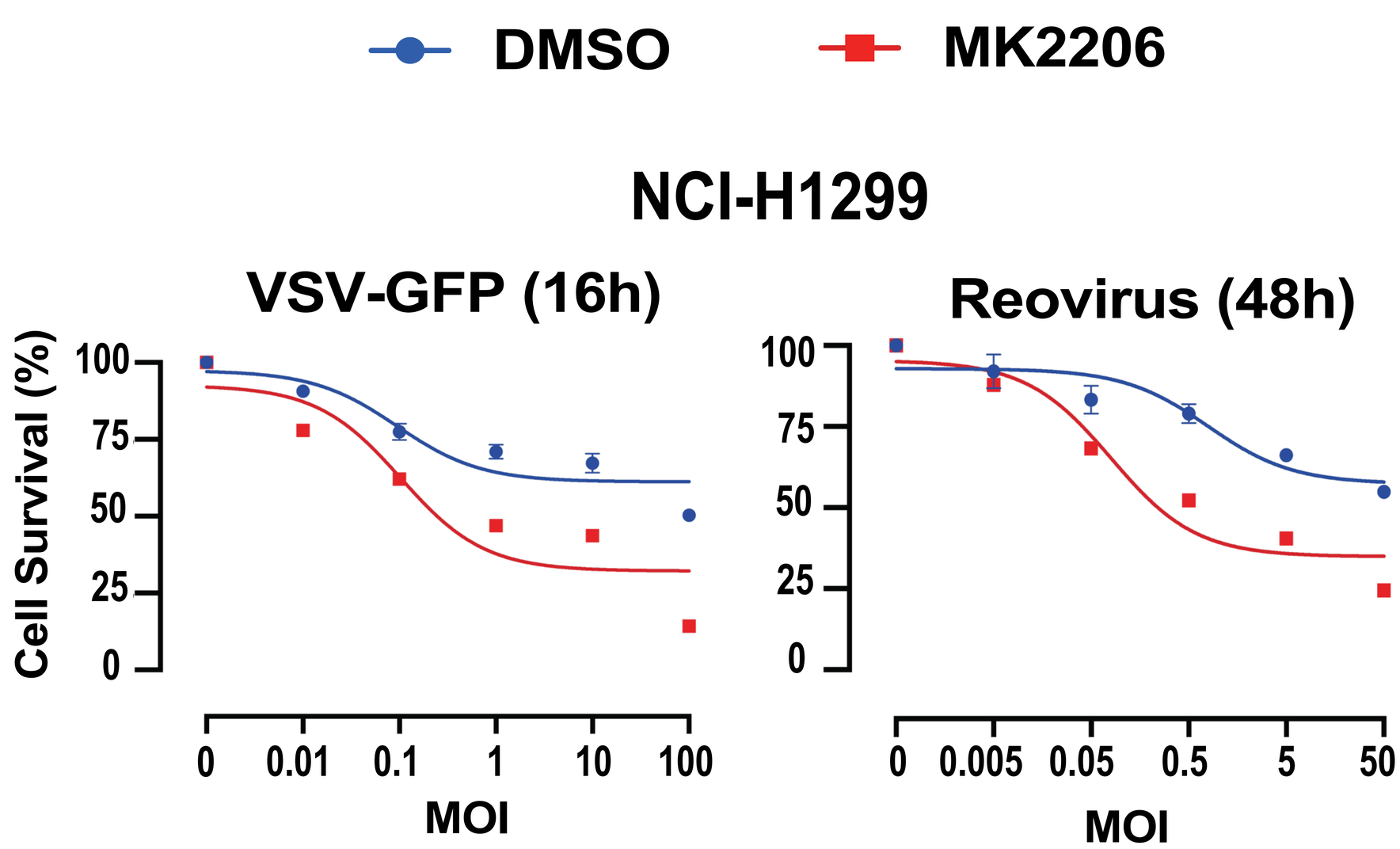
DMSO
MK2206
NCI-H1299
VSV-GFP (16h)
Reovirus (48h)
Cell Survival (%)
100
75
50
25
0
0
0.01
0.1
1
10
100
MOI
0
0.005
0.05
0.5
5
50
MOI

C

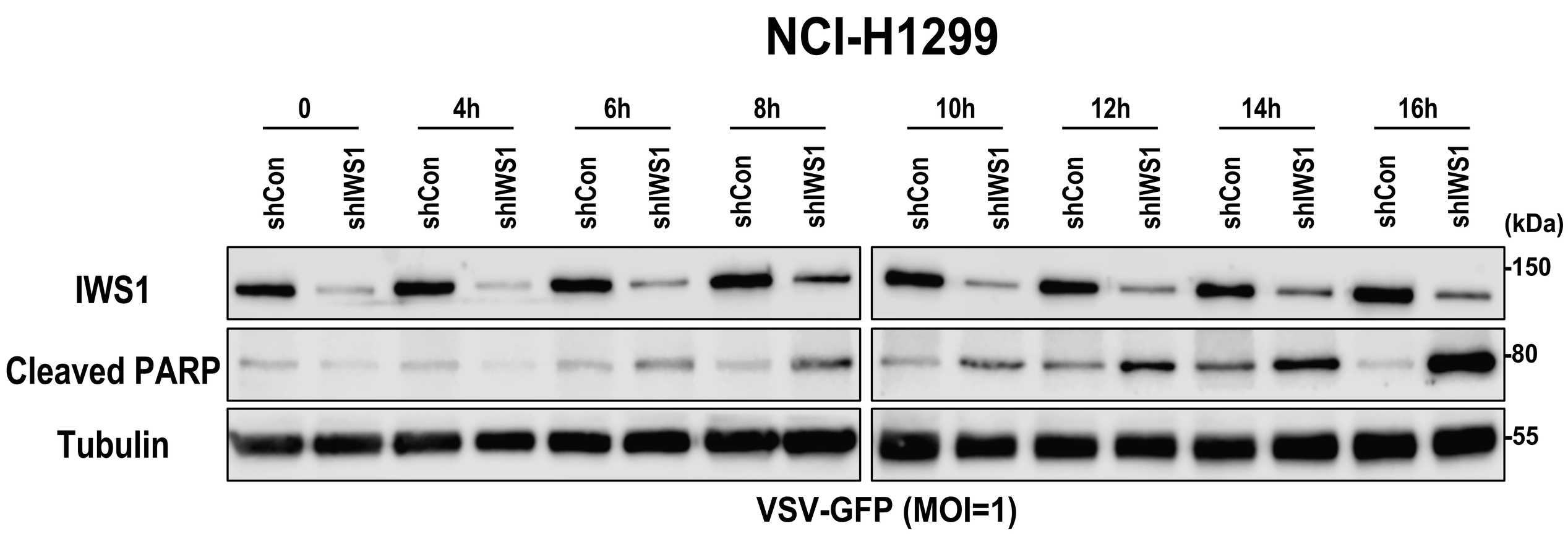
NCI-H1299
0
4h
6h
8h
10h
12h
14h
16h
shCon
shIWS1
(kDa)
IWS1
Cleaved PARP
Tubulin
150
80
55
VSV-GFP (MOI=1)

Figure S7 (Relative to Figure 7). Inhibition of the AKT/p-IWS1 axis sensitizes lung adenocarcinoma cells to oncolytic viral killing.

A. *The loss of IWS1 phosphorylation sensitizes lung adenocarcinoma cells to oncolytic viral killing.* NCI-H1299 cells transduced with the indicated constructs were exposed to increasing MOI of VSV-GFP or Reovirus for 16h and 48h, respectively. Cell proliferation was assessed by fluorescent detection of the reduction of resazurin to resorufin by viable cells and expressed as a percentage of uninfected cells. Mean values are shown ±SD (n=3), data are representative of two independent experiments.

B. *The loss of AKT/p-IWS1 axis sensitizes lung adenocarcinoma cells to oncolytic viral killing.* NCI-H1299 cells treated with DMSO or 5μM of the pan-AKT inhibitor MK2206, were exposed to increasing MOI of VSV-GFP or Reovirus for 16h and 48h, respectively. Cell proliferation was assessed by fluorescent detection of the reduction of resazurin to resorufin by viable cells and expressed as a percentage of uninfected cells. Mean values are shown ±SD (n=3), data are representative of two independent experiments.

C. *The loss of IWS1 phosphorylation sensitizes lung adenocarcinoma cells to oncolytic viral killing via Caspase-mediated death.* NCI-H1299 shControl and shIWS1 cells were infected for the indicated time point intervals with VSV-GFP at a MOI=1. Western blot lysates from these time points were probed with the indicated antibodies, showing a robust cleavage of PARP, a sensitive marker of Caspase mediated apoptosis, in shIWS1 cells even in early time points of infections.